Journal of Scientific Computing manuscript No.
(will be inserted by the editor)

On the Choice of Robin Parameters for the Optimized Schwarz Method for Domains with Non-Conforming Heterogeneities

Yaguang Gu · **Felix Kwok**

Received: date / Accepted: date

Abstract We consider the solution of $-\nabla \cdot (\nu(x)\nabla u) = 0$ by a non-overlapping optimized Schwarz domain decomposition method, where the subdomains do not align with jumps in the coefficient $\nu(x)$. Such a decomposition can be of interest when the jumps are geometrically complex and/or an artifact of the measured data, in which case one would often prefer a simpler decomposition that disregards the location of the discontinuities. For analysis purposes, we focus on a model problem where the diffusivity is piecewise constant, and we analyze the convergence of optimized Schwarz for the two-subdomain case. We consider using either a constant Robin parameter along the whole interface, or a parameter that is scaled proportionally to the local diffusivity. We show that the convergence rate is not robust with respect to the heterogeneity ratio when a constant Robin parameter is used; however, using a scaled Robin parameter restores robustness. We then derive optimal scaling parameter and the corresponding convergence factor. Numerical examples show that this choice also leads to robust convergence behaviour for cases not covered by the analysis.

Keywords domain decomposition methods · optimized Schwarz methods · heterogeneous problems · discontinuous coefficients

Mathematics Subject Classification (2010) 65N55 · 65F10 · 65N22

1 Introduction

Optimized Schwarz methods (OSM) first gained interest among researchers three decades ago, when Lions used Robin interface conditions to overcome the non-convergence of classical Schwarz methods when the subdomains do not overlap [20]. The method was then extended into a class of Schwarz methods called optimized Schwarz methods, where more general transmission conditions are considered on the artificial interfaces. Optimized Schwarz

Yaguang Gu
School of Mathematical Sciences, and College of Oceanic and Atmospheric Sciences, Ocean University of China, Qingdao, Shandong, People's Republic of China
E-mail: guyaguang@ouc.edu.cn

Felix Kwok
Département de mathématiques et de statistique, Université Laval, Québec, Canada
E-mail: felix.kwok@mat.ulaval.ca

methods have been analyzed for the diffusion equations, Helmholtz equations, convection-diffusion equations, etc.; see [24, 25, 19, 12, 9] and references therein. More recently, the methods have also been applied to nonlinear problems [4, 2, 3, 17], and optimized transmission conditions have been used to design a nonlinear preconditioner for dealing with problems with strong local nonlinearities [16].

The choice of Robin parameters in the optimized transmission conditions has a huge impact on the speed of convergence of the algorithm. Indeed, much work has been devoted to analyzing the optimal choice of parameters for specific model problems, see for instance [12, 1, 7]. In this paper, we are particularly interested in elliptic problems of the form $-\nabla\cdot(\nu(x)\nabla u)=0$, where the diffusivity ν can be discontinuous and/or highly oscillatory. When ν is piecewise constant, a natural idea is to align the subdomains with the discontinuity to obtain a nonoverlapping domain decomposition; see the systematic analysis in [10, 26] for the OSM applied to the diffusion problem. More generally, the authors of [15] analyzed the case when the diffusivity consists of piecewise countinuous functions $\nu^-\alpha(x)$ and $\nu^+\alpha(x)$ respectively, where $\alpha(x)\in L^\infty(\Omega)$ is a continuous function bounded away from zero. See also the analysis in [22, 23] for the diffusion equation and [14] for the advection-diffusion equation.

We point out, however, that there are situations where it is impractical or impossible to align the subdomains boundaries to discontinuities in the diffusivity. One example is in oil reservoir simulation, where ν is often highly oscillatory and given by data that is piecewise constant per control volume/element [5]. The discontinuities are thus numerous, geometrically complex, and may not represent meaningful changes in solution behaviour. In these problems, it seems more reasonable to ignore the discontinuities and use a geometrically simpler decomposition, such as into strips or an orthogonal subdivision into $M\times N$ subdomains. In these cases, it is natural to let Robin parameters to vary along the interface, in order to adapt to jumps in the diffusivity within the subdomain.

For analysis purposes, we consider in this paper a diffusion problem with piecewise constant diffusivity ν^- and ν^+ (where we assume without loss of generality that $\nu^-<\nu^+$). To model subdomains that do not align with discontinuities in ν, we consider a decomposition into two subdomains with an interface that is perpendicular to the discontinuity. We then apply Robin transmission conditions to communicate subdomain errors. Note that the convergence of optimized Schwarz methods, even with more general positive definite transmission conditions, has been proved in the sense of H^1-norm; see [6, 8] and references therein. Moreover, it was proved in [21] that for two subdomains separated by an interface with essentially arbitrary geometry, a Robin parameter choice of $\mathcal{O}(h^{-1/2})$ leads to a contraction factor of $1-\mathcal{O}((H/h)^{-1/2})$. However, when the diffusivity $\nu(x)$ varies in space, the constant hidden in the big-O notation generally depends on the heterogeneity ratio ν^+/ν^-. In this paper, we will derive the convergence rate for two possible choices of the Robin parameter: 1) a uniform Robin parameter along the artificial interface, 2) a spatially varying Robin parameter, scaled so that it is proportional to the diffusivity along the artificial interface. We will show that the first choice is not robust with respect to the heterogeneity ratio ν^+/ν^-, whereas with the second choice, one can achieve the classical contraction factor of $1-\mathcal{O}((H/h)^{-1/2})$ with a hidden constant that is independent of the heterogeneity ratio.

The rest of this paper is organized as follows. We introduce the model problem and derive the discrete formulation in Section 2. We then derive in Section 3 the convergence rates of the zeroth order optimized Schwarz method with two different choices of Robin parameters separately; we also provide asymptotic expressions for the optimal Robin parameter for these two choices. In Section 4, we extend our analysis to three dimensions, where we will see that the same asymptotic expressions as those derived in two dimensions hold in the 3D

case. In Section 5, numerical examples show that the proposed scaled Robin parameter is also robust for more general heterogeneous problems not covered by the theory. We finally conclude our work in Section 6. A few useful lemmas involving Sobolev-type estimates are included in Appendix A; these lemmas will be used in the analysis in Sections 3 and 4.

2 Model Problem for Convergence Analysis

2.1 Continuous and Finite Element Formulation

Let $H > 0$ and $\Omega = (-H,H) \times (-H,H)$ be a domain in $\mathbb{R}^2$. In this paper, we consider the following model problem

$$\begin{cases} -\nabla \cdot (\nu(x)\nabla u) = f & \text{in } \Omega, \\ u = g & \text{on } \bar{\Gamma} = \partial\Omega, \end{cases} \tag{1}$$

where

$$\nu(x) = \begin{cases} \nu^- & \text{in } (-H,H) \times (0,H), \\ \nu^+ & \text{in } (-H,H) \times (-H,0), \end{cases}$$

with $\nu^+ > \nu^- > 0$. We look at a decomposition of the physical domain into two non-overlapping subdomains

$$\Omega_1 = (-H,0) \times (-H,H), \qquad \Omega_2 = (0,H) \times (-H,H).$$

In this way, the artificial interface is across the discontinuity of the diffusivity rather than being aligned with it, which leads to subdomains with non-conforming heterogeneities.

Given a set of initial guesses u_1^0 and u_2^0 on Ω_1 and Ω_2 respectively, we solve (1) by the zeroth order optimized Schwarz method:

$$\begin{cases} -\nabla \cdot (\nu(x)\nabla u_i^{n+1}) = f & \text{in } \Omega_i, \\ u_i^{n+1} = g & \text{on } \bar{\Gamma}, \\ \left(\nu(x)\dfrac{\partial}{\partial \mathbf{n}_i} + p_i(x)\right) u_i^{n+1} = \left(\nu(x)\dfrac{\partial}{\partial \mathbf{n}_i} + p_i(x)\right) u_{3-i}^n & \text{on } \Gamma = \bar{\Omega}_1 \cap \bar{\Omega}_2, \end{cases} \tag{2}$$

where $\mathbf{n}_i$ is the unit outer normal vector on the artificial interface of Ω_i, and $p_i(x)$ is the Robin parameter for Ω_i, allowed to vary along the artificial interface. Since the underlying problem is linear, it suffices for us to consider the homogeneous case, i.e., $f = 0$ and $g = 0$, and to look at the convergence of $\{u_i^n\}$ to zero.

We now derive the formulation of the zeroth order optimized Schwarz method for (2) at the discrete level. Using Green's formula for the governing equation in (2), we have

$$\int_{\Omega_i} \nu(x)\nabla u_i^{n+1} \cdot \nabla \psi \, dx - \int_\Gamma \nu(x) \frac{\partial u_i^{n+1}}{\partial \mathbf{n}_i} \psi \, d\Gamma = 0, \quad \text{for all } \psi \in H^1(\Omega_i) \text{ such that } \psi = 0 \text{ on } \bar{\Gamma}.$$

Imposing the boundary condition, we obtain

$$\int_{\Omega_i} \nu(x)\nabla u_i^{n+1} \cdot \nabla \psi \, dx + \int_\Gamma p_i(x) u_i^{n+1} \psi \, d\Gamma = -\int_{\Omega_{3-i}} \nu(x)\nabla u_{3-i}^n \cdot \nabla \psi \, dx + \int_\Gamma p_i(x) u_{3-i}^n \psi \, d\Gamma. \tag{3}$$

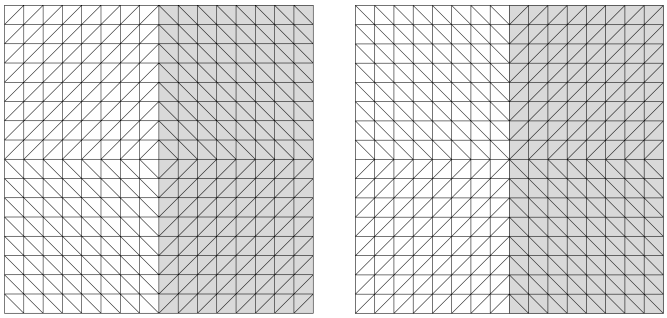

Fig. 1 Centrosymmetric triangular mesh.

We use the P^1 finite element method to discretize (3), obtaining

$$\tilde{A}_{\nu,i}\mathbf{u}_i^{n+1} := (A_{\nu,i} + hL_i)\mathbf{u}_i^{n+1} = B_i\mathbf{u}_{3-i}^n, \quad i = 1,2, \tag{4}$$

where $A_{\nu,i}$ is the stiffness matrix for the first term in (3), L_i is assumed to be a diagonal matrix with its entries being zero everywhere except for those corresponding to the nodes on the artificial interface, due to the second integral in (3), and the matrix B_i assembled from the right-hand side of (3) extracts Robin contributions from the neighbouring subdomain. We note that the assumption for L_i makes sense if the second integral in (3) is computed numerically by a lumped integration, see [18, §7.3.2]. In [13], the authors showed that with this lumped integration rather than the consistent one (the one with accurate integration), optimized Schwarz methods achieve faster convergence. Once lumped integration is applied, the non-zero entries of L_i are exactly Robin parameters at the nodes on the artificial interface. Let R_i be the restriction operator from the set of degrees of freedom in Ω to that in Ω_i, and let R_i^T be the corresponding prolongation operator. Then we have the following concrete expression of B_i:

$$B_i := hL_iR_iR_{3-i}^T - R_iR_{3-i}^TA_{\nu,3-i};$$

see also details in [11].

2.2 Symmetry Assumptions and Substructured Formulation

To facilitate analysis, we make some additional geometric assumptions on our model problem, so that the iteration (4) can be rewritten in a substructured form that simplifies in our convergence analysis later. We assume that our problem is discretized using a centrosymmetric triangular mesh; see possible choices in Figure 1. Since the mesh and the underlying problem are symmetric with respect to y-axis, it is possible to order the local nodes in a symmetric way so that

$$A_\nu = A_{\nu,1} = A_{\nu,2}, \quad L = L_1 = L_2.$$

Moreover, we can order the unknowns in $\mathbf{u}_1^n$ and $\mathbf{u}_2^n$ in order to separate the interior nodes (nodes not on the y-axis) from the interface nodes (nodes on the y-axis), so that

$$\mathbf{u}_i^n = \begin{bmatrix} \mathbf{u}_{i,I}^n \\ \mathbf{u}_{i,\Gamma}^n \end{bmatrix}, \qquad i\text{=}1,2,$$

and

$$A_\nu = \begin{bmatrix} A_{\nu,\mathrm{II}} & A_{\nu,\mathrm{I}\Gamma} \\ A_{\nu,\Gamma\mathrm{I}} & A_{\nu,\Gamma\Gamma} \end{bmatrix}, \qquad L = \begin{bmatrix} 0 & 0 \\ 0 & \hat{L} \end{bmatrix},$$

where the subscripts I and Γ correspond to the interior and interface nodes, respectively, and $\hat{L}$ is a diagonal matrix with size equal to the number of interface degrees of freedom, and whose entries correspond to Robin parameters at the interface nodes. Then the iteration (4) can be written as

$$\begin{bmatrix} A_{\nu,\mathrm{II}} & A_{\nu,\mathrm{I}\Gamma} \\ A_{\nu,\Gamma\mathrm{I}} & A_{\nu,\Gamma\Gamma} + h\hat{L} \end{bmatrix} \begin{bmatrix} \mathbf{u}_{i,I}^{n+1} \\ \mathbf{u}_{i,\Gamma}^{n+1} \end{bmatrix} = \begin{bmatrix} 0 & 0 \\ -A_{\nu,\Gamma\mathrm{I}} & -A_{\nu,\Gamma\Gamma} + h\hat{L} \end{bmatrix} \begin{bmatrix} \mathbf{u}_{3-i,I}^{n} \\ \mathbf{u}_{3-i,\Gamma}^{n} \end{bmatrix}$$

Note that the first block row says

$$A_{\nu,\mathrm{II}}\mathbf{u}_{i,I}^{n+1} + A_{\nu,\mathrm{I}\Gamma}\mathbf{u}_{i,\Gamma}^{n+1} = 0,$$

which is valid for $n = 0, 1, 2, \ldots$ and $i = 1, 2$. Therefore, for $n \geq 1$, we can eliminate the interior degrees of freedom $\mathbf{u}_{i,I}^{n}$ and obtain

$$(h\hat{L} + S_\nu)\mathbf{u}_{i,\Gamma}^{n+1} = (h\hat{L} - S_\nu)\mathbf{u}_{3-i,\Gamma}^{n},$$

where $S_\nu = A_{\nu,\Gamma\Gamma} - A_{\nu,\Gamma\mathrm{I}}A_{\nu,\mathrm{II}}^{-1}A_{\nu,\mathrm{I}\Gamma}$ is the Schur complement. Thus, to study how $\mathbf{u}_i^n$ converges to zero, it suffices to study the spectral radius of the matrix

$$M_\nu = (h\hat{L} + S_\nu)^{-1}(h\hat{L} - S_\nu). \tag{5}$$

Assuming that the diagonal entries of $\hat{L}$ are positive (so that $\hat{L}^{1/2}$ exists and is invertible), we see that

$$\begin{aligned} \rho(M_\nu) &= \rho\left(\hat{L}^{-1/2}S_\nu(h\hat{L} + S_\nu)^{-1}\hat{L}^{1/2}\hat{L}^{-1/2}(h\hat{L} - S_\nu)S_\nu^{-1}\hat{L}^{1/2}\right) \\ &= \rho\left((h\hat{L}^{1/2}S_\nu^{-1}\hat{L}^{1/2} + I)^{-1}(h\hat{L}^{1/2}S_\nu^{-1}\hat{L}^{1/2} - I)\right) = \rho\left((I - G)(I + G)^{-1}\right), \end{aligned}$$

where $G = h\hat{L}^{1/2}S_\nu^{-1}\hat{L}^{1/2}$ is symmetric positive definite, and hence has positive eigenvalues. We are now ready to state a first convergence result.

Theorem 1 *Let the initial guesses $\mathbf{u}_1^0$ and $\mathbf{u}_2^0$ be given. The subdomain solutions $\mathbf{u}_i^n$ generated by the optimized Schwarz method* (4) *converge to zero provided that all the non-zero entries of diagonal matrix $\hat{L}$ are positive.*

Proof Since M_ν has the same spectral radius as $(I - G)(I + G)^{-1}$, it suffices to show that the eigenvalues of $(I - G)(I + G)^{-1}$ are less than 1 in absolute value. We have seen that all the eigenvalues of G are positive; let $\lambda_i > 0$ be the i-th largest eigenvalue of G, for $i = 1, 2, \ldots, n$. Then the i-th largest eigenvalue of $(I - G)(I + G)^{-1}$, denoted by μ_i, is given by

$$\mu_i = \frac{1 - \lambda_{n+1-i}}{1 + \lambda_{n+1-i}};$$

since $\lambda_{n+1-i} > 0$, we must have $|\mu_i| < 1$ for all i, so $\rho(M_\nu) < 1$.

3 Optimization of Robin Parameters

In order to study the choice of Robin parameters along the interface, let us further classify the interface nodes as follows:

1. interface nodes on the top half of Γ (indexed by the subscript '1');
2. interface node at $(0,0)$ (indexed by the subscript '$*$');
3. interface nodes on the bottom half of Γ (indexed by the subscript '2').

Partitioning the matrix S_ν correspondingly yields

$$S_\nu = A_{\nu,\Gamma\Gamma} - A_{\nu,\Gamma\mathrm{I}} A_{\nu,\mathrm{II}}^{-1} A_{\nu,\mathrm{I}\Gamma} = \begin{bmatrix} S_{11} & S_{1*} & S_{12} \\ S_{*1} & S_{**} & S_{*2} \\ S_{21} & S_{2*} & S_{22} \end{bmatrix}.$$

3.1 Two Choices of $\hat{L}$

We have proved the convergence of the discrete zeroth order optimized Schwarz method. In this section, we will discuss two choices of $\hat{L}$. Note that different choices lead to different convergence rates.

One possible choice is that we use uniform Robin parameter everywhere along the artificial interface Γ, i.e., $\hat{L} = pI$. In that case, $G = hpS_\nu^{-1}$, so it is simply a scaled version of the inverse of the Schur complement.

We now introduce another possible choice of $\hat{L}$. In [10], authors proved that for problems with constant diffusivity, the optimal Robin parameter should be proportional to the diffusion coefficient. For our model, we can observe that in each half of the physical domain Ω, i.e., in the top half or in the bottom half of Ω, the diffusivity is constant. This observation gives us an idea of choosing the Robin parameter to be proportional to the diffusivity, i.e.,

$$\hat{L} = pD := p \begin{bmatrix} \nu^- I & & \\ & \nu^* & \\ & & \nu^+ I \end{bmatrix},$$

where ν^* is the Robin parameter for the node at the discontinuity and will be discussed later.

In both cases, our aim is to choose the parameter p to minimize the spectral radius of $(I-G)(I+G)^{-1}$, which means that we need to consider the min-max problem of the form

$$\min_p \max_i \left| \frac{1-\lambda_i(G)}{1+\lambda_i(G)} \right| = \min_p \max_i \left| \frac{1-hp\lambda_i(Z^{-1})}{1+hp\lambda_i(Z^{-1})} \right|, \tag{6}$$

where $Z = S_\nu$ for $\hat{L} = pI$, and $Z = D^{-1/2} S_\nu D^{-1/2}$ for $\hat{L} = pD$.

Theorem 2 *Let $[\beta_{\min}, \beta_{\max}] \subset (0,\infty)$ be any interval containing the spectrum of Z. Then the choice*

$$p^* = \frac{\sqrt{\beta_{\min}\beta_{\max}}}{h} \tag{7}$$

leads to a convergence factor of

$$\rho(M_\nu) \le \frac{1-(\beta_{\min}/\beta_{\max})^{1/2}}{1+(\beta_{\min}/\beta_{\max})^{1/2}} \le 1 - \sqrt{\beta_{\min}/\beta_{\max}}. \tag{8}$$

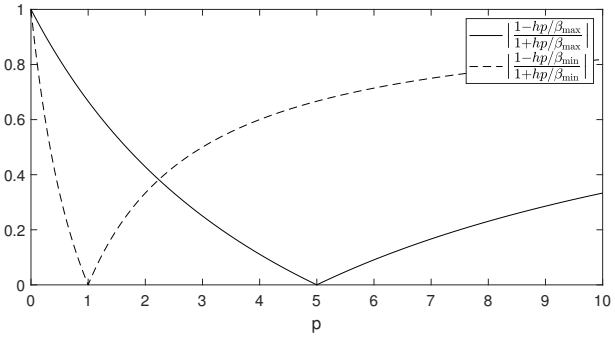

Fig. 2 Determining the optimal parameter p for given eigenvalues $\beta_{\min}$ and $\beta_{\max}$ of the matrix Z.

Additionally, if $\beta_{\min} = \lambda_{\min}(Z)$ and $\beta_{\max} = \lambda_{\max}(Z)$, then the first inequality in (8) *is tight, and the choice* (7) *is the optimal one that solves the min-max problem* (6)*.*

Proof The argument is classical and similar to the one for determining the optimal parameter for Richardson iterations, see [27, Example 4.1]. The eigenvalues of $(I-G)(I+G)^{-1}$ all lie between $\dfrac{1-hp/\lambda_{\min}(Z)}{1+hp/\lambda_{\min}(Z)} \geq \dfrac{1-hp/\beta_{\min}}{1+hp/\beta_{\min}}$ and $\dfrac{1-hp/\lambda_{\max}(Z)}{1+hp/\lambda_{\max}(Z)} \leq \dfrac{1-hp/\beta_{\max}}{1+hp/\beta_{\max}}$. This suggests that we choose p that minimizes $\max\left\{\left|\dfrac{1-hp/\beta_{\min}}{1+hp/\beta_{\min}}\right|, \left|\dfrac{1-hp/\beta_{\max}}{1+hp/\beta_{\max}}\right|\right\}$, i.e., when

$$-\frac{1-hp/\beta_{\min}}{1+hp/\beta_{\min}} = \frac{1-hp/\beta_{\max}}{1+hp/\beta_{\max}}, \tag{9}$$

see Figure 2. The solution p^* of (9) satisfies $\dfrac{hp^*}{\beta_{\min}} \cdot \dfrac{hp^*}{\beta_{\max}} = 1$, so plugging this solution into the maximum leads to the estimate (8). Moreover, if the interval $[\beta_{\min}, \beta_{\max}]$ is tight, then any other choice of p will lead to an increase in the maximum, so the choice in (7) is optimal and solves the min-max problem (6), as required. □

Theorem 2 implies that the smaller the condition number $\kappa(Z) = \lambda_{\max}(Z)/\lambda_{\min}(Z)$ of Z, the faster the Robin iteration converges to the exact solution. Therefore, if we can estimate the condition number of Z for our two choices of $\hat{L}$, i.e., for $Z = S_\nu$ or $Z = D^{-1/2} S_\nu D^{-1/2}$, we can deduce the speed of convergence of our Robin method. We now state the two main results of this section.

Theorem 3 *For the choice $\hat{L} = pI$ with the Robin parameter satisfying*

$$p = p_1^* = \mathscr{O}\left(\sqrt{\frac{\nu^- \nu^+}{Hh}}\right), \tag{10}$$

the contraction factor of the method is bounded by

$$\rho\left(M_\nu\right) \leq 1 - C\sqrt{\frac{\nu^- h}{\nu^+ H}}, \tag{11}$$

where $C > 0$ is independent of the mesh parameter h, the size of the domain H, and the diffusivities ν^-, ν^+.

Theorem 4 *For the choice $\hat{L} = p \cdot \mathrm{diag}(\nu^- I, \nu^*, \nu^+ I)$, let ν^* be chosen such that $\nu^- + \nu^+ < C_* \nu^*$ for some constant C_* independent of the mesh parameter h and the coefficients ν^-, ν^+. Then choosing the optimal parameter $p = p_\nu^*$ to have the asymptotic expression*

$$p_\nu^* = \mathscr{O}\left(\frac{1}{\sqrt{Hh}}\right), \tag{12}$$

leads to a contraction factor of the method that is bounded by

$$\rho(M_\nu) \leq 1 - C\sqrt{\frac{h}{H}},$$

where $C > 0$ is independent of the mesh parameter h, the size of the domain H, and the diffusivities ν^-, ν^+.

In other words, choosing the Robin parameters to be proportional to the diffusivity makes the Robin method robust with respect to the contrast in coefficients, which is not the case for a uniform Robin parameter. The remainder of the section is devoted to proving these two results, with the help of Sobolev-type estimates applied to discrete harmonic extensions. A list of useful Sobolev estimates is given in Appendix A.

3.2 Spectral Analysis

Since our analysis will rely heavily on discrete harmonic extensions, we introduce here various notations related to such extensions. Let $\hat{\Omega} \subset \mathbb{R}^2$ be a bounded region with boundary $\hat{\Gamma} := \partial\hat{\Omega}$. (Later on, $\hat{\Omega}$ will be part of the domain Ω, and $\hat{\Gamma}$ will be the interface between $\hat{\Omega}$ and the rest of the domain.) Consider the bilinear form defined on $H^1(\hat{\Omega})$,

$$a(u,v) = \int_{\hat{\Omega}} a(x)\nabla u \cdot \nabla v \, dx,$$

where $0 < a_{\min} \leq a(x) \in L^\infty(\hat{\Omega})$. Let u and v be piecewise linear finite element functions defined on $\hat{\Omega}$, so that they can be represented by the vectors $\mathbf{u}$ and $\mathbf{v}$ of their degrees of freedom at the nodes.[1] Then $a(u,v) = \mathbf{v}^T \hat{A} \mathbf{u}$, where

$$\hat{A} = \begin{bmatrix} \hat{A}_{\mathrm{II}} & \hat{A}_{\mathrm{I}\hat{\Gamma}} \\ \hat{A}_{\hat{\Gamma}\mathrm{I}} & \hat{A}_{\hat{\Gamma}\hat{\Gamma}} \end{bmatrix}$$

is the stiffness matrix corresponding to $a(\cdot,\cdot)$, suitably partitioned to distinguish the boundary nodes (those on $\hat{\Gamma}$) from the interior ones (everything else).

Now let $u_{\hat{\Gamma}}$ be the trace of a finite element function on $\hat{\Gamma}$, and $\mathbf{u}_{\hat{\Gamma}}$ be its associated vector. Then a vector $\mathbf{u} = (\mathbf{u}_{\mathrm{I}}^T, \mathbf{u}_{\hat{\Gamma}}^T)^T$ is called the discrete $a(x)$-harmonic extension of $\mathbf{u}_{\hat{\Gamma}}$ into $\hat{\Omega}$ if

$$\hat{A}_{\mathrm{II}}\mathbf{u}_{\mathrm{I}} + \hat{A}_{\mathrm{I}\hat{\Gamma}}\mathbf{u}_{\hat{\Gamma}} = 0.$$

Note that since $\hat{A}_{II}$ is invertible, there is a unique discrete $a(x)$-harmonic extension for any given $\mathbf{u}_{\hat{\Gamma}}$, which we denote by $\mathscr{H}_a(\mathbf{u}_{\hat{\Gamma}})$. The main tool that will be used repeatedly in our analysis is the fact that discrete harmonic extensions has the smallest energy norm among all finite element functions that have the same boundary trace $\mathbf{u}_{\hat{\Gamma}}$:

[1] In the rest of this paper, we will use normal letters, e.g., u, to denote finite element functions or their traces on the boundary, and use bold letters, e.g., $\mathbf{u}$, to denote the vector corresponding to u. We will often switch between normal and bold letters.

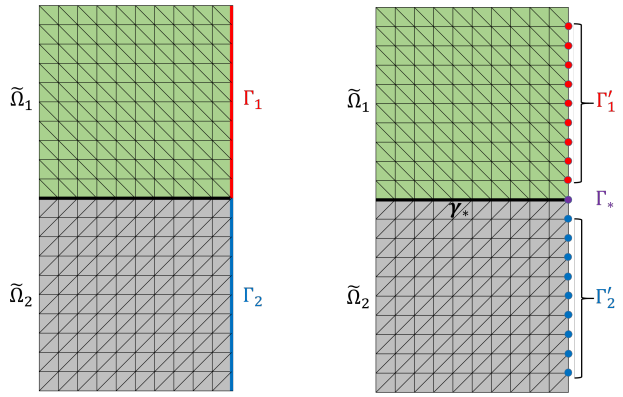

Fig. 3 Notations for different portions of the subdomain and the interface, in the continuous and discrete settings.

Lemma 1 ([28], Lemma 4.9) *Let* $\mathbf{u} = \mathscr{H}_a(\mathbf{u}_{\hat{\Gamma}})$ *be the discrete* $a(x)$*-harmonic extension of* $\mathbf{u}_{\hat{\Gamma}}$*. Let* $\hat{S} := \hat{A}_{\hat{\Gamma}\hat{\Gamma}} - \hat{A}_{\hat{\Gamma}I}\hat{A}_{II}^{-1}\hat{A}_{I\hat{\Gamma}}$ *be the Schur complement of* $\hat{A}$ *after eliminating the interior nodes. Then*

$$\mathbf{u} = \arg\min a(v,v) = \arg\min \mathbf{v}^T\hat{A}\mathbf{v},$$
$$s.t. \quad v \in P^1, \quad v|_\Gamma = u_{\hat{\Gamma}},$$

and

$$\mathbf{u}_{\hat{\Gamma}}^T\hat{S}\mathbf{u}_{\hat{\Gamma}} = \mathbf{u}^T\hat{A}\mathbf{u}.$$

Next, we return to the centro-symmetric model problem and introduce some notation related to the geometry of the subdomains, see Figure 3.

1. The top half and the bottom half of Ω_1 are denoted by $\tilde{\Omega}_1$ and $\tilde{\Omega}_2$, respectively. The corresponding artificial interfaces are denoted by $\Gamma_1 = \partial\tilde{\Omega}_1 \cap \Gamma$ and $\Gamma_2 = \partial\tilde{\Omega}_2 \cap \Gamma$, respectively. Denote $\gamma_* = \partial\tilde{\Omega}_1 \cap \partial\tilde{\Omega}_2$.
2. The nodes that lie on the top half of the artificial interface are plotted in red. The corresponding set of interface nodes is denoted by Γ_1'. The nodes that lie on the bottom half of the artificial interface are plotted in blue. The corresponding set of interface nodes is denoted by Γ_2'. The node that lies in the middle is plotted in purple and is denoted by Γ_*.

Note that for our model, the iterates are always zero on the physical boundary. As long as we are given a trace function u_Γ on the artificial interface Γ, we know the whole trace on $\partial\Omega_1$. Therefore, we will omit the nodes on $\partial\Omega_1 \setminus \Gamma$ and still use the notation $\mathscr{H}_a(\mathbf{u}_\Gamma)$ to denote the discrete harmonic extension. The subscript a will change based on the inner product considered.

3.2.1 Spectrum of $Z^{-1} = S_\nu$

First, consider the homogenous case $a(x) = 1$. The inner product becomes

$$a_1(u,v) = \int_{\Omega_1} \nabla u \cdot \nabla v \, dx. \tag{13}$$

Denote the stiffness matrix associated to the scalar product in (13) and the corresponding Schur complement matrix by A_1 and S_1, respectively. Given a trace u_Γ on Γ, we define

$\mathbf{u_1} = \mathscr{H}_1(\mathbf{u}_\Gamma)$ as the discrete 1-harmonic extension of $\mathbf{u}_\Gamma$ associated with the inner product defined in (13). Then by Lemma 1 we know that

$$\begin{aligned} \mathbf{u}_1 = \arg\min a_1(u,u) = \arg\min \mathbf{u}^T A_1 \mathbf{u}, \\ \text{s.t.} \quad u \in P^1, \quad u|_\Gamma = u_\Gamma, \end{aligned}$$

and

$$\mathbf{u}_\Gamma^T S_1 \mathbf{u}_\Gamma = \mathbf{u}_1^T A_1 \mathbf{u}_1.$$

Next, consider our model $a(x) = \nu(x)$, where ν is piecewise constant on each of $\tilde{\Omega}_1$ and $\tilde{\Omega}_2$. The inner product becomes

$$a_\nu(u,u) = \int_{\Omega_1} \nu(x) \nabla u \cdot \nabla u \, dx = \nu^- \int_{\tilde{\Omega}_1} \nabla u \cdot \nabla u \, dx + \nu^+ \int_{\tilde{\Omega}_2} \nabla u \cdot \nabla u \, dx. \tag{14}$$

Note that $\nu^- a_1(u,u) \le a_\nu(u,u) \le \nu^+ a_1(u,u)$ for any P_1 function u. Similarly to the above, we denote the stiffness matrix to (14) and the corresponding Schur complement matrix by A_ν and S_ν, respectively. By the same reasoning as above, for any trace function u_Γ on the interface, the discrete ν-harmonic extension $\mathbf{u}_\nu = \mathscr{H}_\nu(\mathbf{u}_\Gamma)$ satisfies

$$\begin{aligned} \mathbf{u}_\nu = \arg\min a_\nu(u,u) = \arg\min \mathbf{u}^T A_\nu \mathbf{u}, \\ \text{s.t.} \quad u \in P^1, \quad u|_\Gamma = u_\Gamma, \end{aligned} \tag{15}$$

and

$$\mathbf{u}_\Gamma^T S_\nu \mathbf{u}_\Gamma = \mathbf{u}_\nu^T A_\nu \mathbf{u}_\nu.$$

We are ready to show our first main result.

Theorem 5 *Let u_Γ be the trace of a finite element function on Γ, and let $\mathbf{u}_\Gamma$ be the vector corresponding to u_Γ. Then their exist constants c and C, independent of h and H, such that*

$$c\nu^- h H^{-1} \mathbf{u}_\Gamma^T \mathbf{u}_\Gamma \le \mathbf{u}_\Gamma^T S_\nu \mathbf{u}_\Gamma \le C\nu^+ \mathbf{u}_\Gamma^T \mathbf{u}_\Gamma, \tag{16}$$

where h is the diameter of the element, and H is the diameter of Ω_i. Thus, there exists a constant C' independent of h, H, ν^- and ν^+ such that

$$\kappa(S_\nu) < C' \frac{\nu^+ H}{\nu^- h}. \tag{17}$$

Proof Let $\mathbf{u_1} = \mathscr{H}_1(\mathbf{u}_\Gamma)$ be the discrete 1-harmonic extension of $\mathbf{u}_\Gamma$ into Ω_1, and let $\mathbf{u}_\nu = \mathscr{H}_\nu(\mathbf{u}_\Gamma)$ be the discrete ν-harmonic extension of $\mathbf{u}_\Gamma$ into Ω_1. For any vector $\mathbf{u}_\Gamma$, since $u_1|_\Gamma = u_\nu|_\Gamma = u_\Gamma$, we have by the energy minimization property

$$\mathbf{u}_\Gamma^T S_\nu \mathbf{u}_\Gamma = \mathbf{u}_\nu^T A_\nu \mathbf{u}_\nu = a_\nu(u_\nu, u_\nu) \le a_\nu(u_1, u_1) \le \nu^+ a_1(u_1, u_1) = \nu^+ \mathbf{u}_1^T A_1 \mathbf{u}_1 = \nu^+ \mathbf{u}_\Gamma^T S_1 \mathbf{u}_\Gamma,$$

and

$$\mathbf{u}_\Gamma^T S_\nu \mathbf{u}_\Gamma = \mathbf{u}_\nu^T A_\nu \mathbf{u}_\nu = a_\nu(u_\nu, u_\nu) \ge \nu^- a_1(u_\nu, u_\nu) \ge \nu^- a_1(u_1, u_1) = \nu^- \mathbf{u}_1^T A_1 \mathbf{u}_1 = \nu^- \mathbf{u}_\Gamma^T S_1 \mathbf{u}_\Gamma.$$

Combining both inequalities, we have $\nu^- \mathbf{u}_\Gamma^T S_1 \mathbf{u}_\Gamma \le \mathbf{u}_\Gamma^T S_\nu \mathbf{u}_\Gamma \le \nu^+ \mathbf{u}_\Gamma^T S_1 \mathbf{u}_\Gamma$. Using Lemma 5, we estimate the terms involving S_1 to obtain

$$c_1 H^{-1} \nu^- \|u\|_\Gamma^2 \le \mathbf{u}_\Gamma^T S_\nu \mathbf{u}_\Gamma \le C_1 \nu^+ h^{-1} \|u\|_\Gamma^2, \tag{18}$$

for some constants c_1 and C_1, independent of h, H, ν^- and ν^+. Then by Lemma 3 on the equivalence of the discrete and continuous L^2 norms, we have

$$c\nu^- hH^{-1}\mathbf{u}_\Gamma^T\mathbf{u}_\Gamma \leq \mathbf{u}_\Gamma^T S_\nu \mathbf{u}_\Gamma \leq C\nu^+\mathbf{u}_\Gamma^T\mathbf{u}_\Gamma,$$

where we have substituted $n=2$ in the Lemma for our two-dimensional case. Therefore, there exists a constant $C' = C/c$, independent of h, H, ν^- and ν^+, such that

$$\kappa(S_\nu) < C'\frac{\nu^+ H}{\nu^- h}.$$

□

The above result leads to an estimate on the eigenvalues of S_ν, which in turn allows us to prove the convergence rate of the Robin iteration stated in Theorem 3.

Proof (Theorem 3) By Theorem 5, the spectrum of $Z = S_\nu$ lies within $[\beta_{1,\min}, \beta_{1,\max}]$, where

$$\beta_{1,\min} = c\nu^- hH^{-1} \quad \text{and} \quad \beta_{1,\max} = C\nu^+.$$

Hence Theorem 2 suggests choosing the parameter

$$p = p_1^* = \frac{1}{h}\sqrt{c\nu^- hH^{-1}\cdot C\nu^+} = \mathscr{O}\left(\sqrt{\frac{\nu^-\nu^+}{Hh}}\right).$$

This choice leads to the condition number of $Z = S_\nu$ being bounded by $\kappa(S_\nu) \leq \frac{C'\nu^+ H}{\nu^- h}$, so Theorem 2 implies that the asymptotic expression of the convergence factor satisfies

$$\rho\left(M_\nu\right) \leq 1 - \sqrt{\frac{\nu^- h}{C'\nu^+ H}}.$$

□

3.2.2 Spectrum of $Z^{-1} = D^{-1/2}S_\nu D^{-1/2}$

We now analyze the spectrum of $Z^{-1} = D^{-1/2}S_\nu D^{-1/2}$ in order to deduce the convergence of the method for the case of spatially-varying Robin parameters. To do so, we need to provide upper and lower bounds for the quantity $\mathbf{u}_\Gamma^T D^{-1/2}S_\nu D^{-1/2}\mathbf{u}_\Gamma$ for any given trace $\mathbf{u}_\Gamma$. For analysis purposes, we will define the *scaled trace* $\mathbf{w}_\Gamma := D^{-1/2}\mathbf{u}_\Gamma$, as well as the discrete ν-harmonic extension of $\mathbf{w}_\Gamma$ into Ω_1, which satisfies

$$\begin{aligned} \mathbf{w}_\nu = \arg\min a_\nu(w,w) &= \arg\min \mathbf{w}^T A_\nu \mathbf{w}, \\ \text{s.t.} \quad w \in P^1, &\quad w|_\Gamma = w_\Gamma. \end{aligned} \tag{19}$$

Here, w_Γ is the trace of the finite element function corresponding to $\mathbf{w}_\Gamma$. With these definitions, we see that

$$\mathbf{u}_\Gamma^T D^{-1/2}S_\nu D^{-1/2}\mathbf{u}_\Gamma = \mathbf{w}_\Gamma S_\nu \mathbf{w}_\Gamma = a_\nu(w_\nu, w_\nu) = \mathbf{w}_\nu A_\nu \mathbf{w}_\nu.$$

Before we prove our second main result, we first show how the matrices A_1 and A_ν are related. Let us rewrite A_1 in block form as:

$$A_1 = \begin{bmatrix} A_{11} & A_{1\gamma} & 0 \\ A_{\gamma 1} & A_{\gamma\gamma} & A_{\gamma 2} \\ 0 & A_{2\gamma} & A_{22} \end{bmatrix}, \tag{20}$$

where the subscripts 1, γ and 2 correspond to the nodes above, on and below the x-axis, respectively. For A_ν with the same ordering, we have the following lemma.

Lemma 2 *Assume that the triangular mesh is centrosymmetric; see examples in Figure 1. Then the block structure representation of the stiffness matrix A_ν is*

$$A_\nu = \begin{bmatrix} A_{\nu,11} & A_{\nu,1\gamma} & 0 \\ A_{\nu,\gamma 1} & A_{\nu,\gamma\gamma} & A_{\nu,\gamma 2} \\ 0 & A_{\nu,2\gamma} & A_{\nu,22} \end{bmatrix} = \begin{bmatrix} \nu^- A_{11} & \nu^- A_{1\gamma} & 0 \\ \nu^- A_{\gamma 1} & \frac{\nu^-+\nu^+}{2} A_{\gamma\gamma} & \nu^+ A_{\gamma 2} \\ 0 & \nu^+ A_{2\gamma} & \nu^+ A_{22} \end{bmatrix}. \tag{21}$$

Proof Since the diffusion coefficient is ν^- in $\tilde{\Omega}_1$ and is ν^+ in $\tilde{\Omega}_2$, the expressions for all sub-blocks except $A_{\nu,\gamma\gamma}$ are obvious. For the sub-block $A_{\nu,\gamma\gamma}$, we can split it into $A_{\nu,\gamma\gamma} = A_{\nu,\gamma\gamma 1} + A_{\nu,\gamma\gamma 2}$, where $A_{\nu,\gamma\gamma 1}$ and $A_{\nu,\gamma\gamma 2}$ are partially assembled stiffness matrices in $\tilde{\Omega}_1$ and $\tilde{\Omega}_2$, respectively. Then we can easily see that $A_{\nu,\gamma\gamma 1} = \nu^- A_{\gamma\gamma 1}$ and $A_{\nu,\gamma\gamma 2} = \nu^+ A_{\gamma\gamma 2}$, where we have used a similar splitting for $A_{\gamma\gamma}$. If the mesh is centrosymmetric, we will immediately have $A_{\nu,\gamma\gamma} = \frac{\nu^-+\nu^+}{2} A_{\gamma\gamma}$. □

Now we are ready to present our second main result.

Theorem 6 *Let ν^* satisfy $\nu^- + \nu^+ < C_* \nu^*$ for some constant C_*, independent of ν^- and ν^+. Then there exist constants c and C, independent of h, H, ν^- and ν^+, such that*

$$chH^{-1}\mathbf{u}_\Gamma^T \mathbf{u}_\Gamma \le \mathbf{u}_\Gamma^T D^{-1/2} S_\nu D^{-1/2} \mathbf{u}_\Gamma \le C\mathbf{u}_\Gamma^T \mathbf{u}_\Gamma. \tag{22}$$

Consequently, there exists a constant C' independent of h, H, ν^- and ν^+ such that

$$\kappa(D^{-1/2} S_\nu D^{-1/2}) < \frac{C'H}{h}. \tag{23}$$

Proof We first derive the lower bound. To do so, we first split the term $\mathbf{u}_\Gamma^T \mathbf{u}_\Gamma$ into a sum of two traces from the upper and lower parts of the interface. Using the definition of the ν-harmonic extension $w_\nu = \mathscr{H}_\nu(w_\Gamma)$, we obtain

$$\mathbf{u}_\Gamma^T \mathbf{u}_\Gamma = \mathbf{u}_{\Gamma_1'}^T \mathbf{u}_{\Gamma_1'} + \mathbf{u}_{\Gamma_2}^T \mathbf{u}_{\Gamma_2} \le c_1 \frac{\nu^-}{h} \|w_\nu\|_{L^2(\Gamma_1)}^2 + c_1' \frac{\nu^+}{h} \|w_\nu\|_{L^2(\Gamma_2)}^2 \tag{24}$$

where the conversion from the discrete ℓ^2 norm to the continuous L^2 norm uses Lemma 3, with constants c_1 and c_1' independent of h, H, ν^- and ν^+. For the first term on the right hand side of (24), we have

$$c_1 \frac{\nu^-}{h} \|w_\nu\|_{L^2(\Gamma_1)}^2 \le c_1 \frac{\nu^-}{h} \left(\|w_\nu\|_{L^2(\Gamma_1)}^2 + \|w_\nu\|_{L^2(\gamma_*)}^2 \right) = c_1 \frac{\nu^-}{h} \|w_\nu\|_{L^2(\partial\tilde{\Omega}_1)}^2. \tag{25}$$

Since w_ν vanishes on the physical boundary, then by Lemma 8 and Lemma 6, we know that there exist constants c_2 and c_3, independent of h, H, ν^- and ν^+, such that

$$c_1 \frac{\nu^-}{h} \|w_\nu\|_{L^2(\partial\tilde{\Omega}_1)}^2 \le c_1 c_2 \frac{H\nu^-}{h} |w_\nu|_{H^{1/2}(\partial\tilde{\Omega}_1)}^2 \le c_1 c_2 c_3 \frac{H\nu^-}{h} |w_\nu|_{H^1(\tilde{\Omega}_1)}^2. \tag{26}$$

Similarly for the second term, we have

$$c_1' \frac{\nu^+}{h} \|w_\nu\|_{L^2(\partial\tilde{\Omega}_2)}^2 \le c_1' c_2' \frac{H\nu^+}{h} |w_\nu|_{H^{1/2}(\partial\tilde{\Omega}_2))}^2 \le c_1' c_2' c_3' \frac{H\nu^+}{h} |w_\nu|_{H^1(\tilde{\Omega}_2)}^2, \tag{27}$$

for some constants c_1', c_2' and c_3', independent of h, H, ν^- and ν^+. Combining (24) and (27), we have

$$\mathbf{u}_\Gamma^T \mathbf{u}_\Gamma \le \max\{c_1 c_2 c_3, c_1' c_2' c_3'\} \frac{H}{h} \mathbf{w}_\nu^T A_\nu \mathbf{w}_\nu. \tag{28}$$

Finally, letting $C = \max\{c_1c_2c_3, c_1'c_2'c_3'\}$ and using the fact that $\mathbf{w}_\nu$ is the ν-harmonic extension of $\mathbf{w}_\Gamma$, we conclude that

$$\frac{CH}{h}\mathbf{w}_\nu^T A_\nu \mathbf{w}_\nu = \frac{CH}{h}\mathbf{w}_\Gamma^T S_\nu \mathbf{w}_\Gamma = \frac{CH}{h}\mathbf{u}_\Gamma^T D^{-1/2} S_\nu D^{-1/2}\mathbf{u}_\Gamma. \tag{29}$$

Therefore, there exists a constant $c = 1/C$, independent of h, H, ν^- and ν^+, such that

$$chH^{-1}\mathbf{u}_\Gamma^T\mathbf{u}_\Gamma \le \mathbf{u}_\Gamma^T D^{-1/2} S_\nu D^{-1/2}\mathbf{u}_\Gamma. \tag{30}$$

We now derive the upper bound. Using the energy minimization property of harmonic extensions, we see that for any finite element function u with $u|_\Gamma = u_\Gamma$, we have

$$\mathbf{u}_\Gamma^T D^{-1/2} S_\nu D^{-1/2}\mathbf{u}_\Gamma \le \mathbf{u}^T \tilde{D}^{-1/2} A_\nu \tilde{D}^{-1/2}\mathbf{u}, \tag{31}$$

where

$$\tilde{D} = \begin{bmatrix} \nu^- I & & \\ & \nu^* I & \\ & & \nu^+ I \end{bmatrix}$$

is a diagonal matrix having the same size and block structures as A_1 and A_ν, but with zero off-diagonal blocks. The matrix $\tilde{D}^{-1/2}A_\nu\tilde{D}^{-1/2}$ can be computed as follows.

$$\begin{aligned}\tilde{D}^{-1/2}A_\nu\tilde{D}^{-1/2} &= \begin{bmatrix} \frac{1}{\sqrt{\nu^-}}I & & \\ & \frac{1}{\sqrt{\nu^*}}I & \\ & & \frac{1}{\sqrt{\nu^+}}I \end{bmatrix} A_\nu \begin{bmatrix} \frac{1}{\sqrt{\nu^-}}I & & \\ & \frac{1}{\sqrt{\nu^*}}I & \\ & & \frac{1}{\sqrt{\nu^+}}I \end{bmatrix} \\ &= \begin{bmatrix} A_{11} & \sqrt{\frac{\nu^-}{\nu^*}}A_{1\gamma} & \\ \sqrt{\frac{\nu^-}{\nu^*}}A_{\gamma 1} & \frac{\nu^-+\nu^+}{2\nu^*}A_{\gamma\gamma} & \sqrt{\frac{\nu^+}{\nu^*}}A_{\gamma 2} \\ & \sqrt{\frac{\nu^+}{\nu^*}}A_{2\gamma} & A_{22} \end{bmatrix}.\end{aligned}$$

The remaining work is to construct an appropriate vector $\mathbf{u}$ that agrees with u_Γ on the interface, so that there is a constant C independent of h, H, ν^- and ν^+ for which the inequality $\mathbf{u}^T\tilde{D}^{-1/2}A_\nu\tilde{D}^{-1/2}\mathbf{u} \le C\mathbf{u}^T\mathbf{u}$ holds. Concretely, we construct the vector $\mathbf{u}$ as follows.

1. Let $\mathbf{u}_1 = \mathscr{H}_{\nu^-}((\mathbf{u}_{\Gamma_1'}^T, \mathbf{0}_{\gamma_*}^T)^T)$ be the discrete ν^--harmonic extension of $(\mathbf{u}_{\Gamma_1'}^T, \mathbf{0}_{\gamma_*}^T)^T$ into $\tilde{\Omega}_1$, associated with the inner product $a_{\nu^-}(u,v) = \nu^-\int_{\tilde{\Omega}_1}\nabla u\cdot\nabla v\,dx$.
2. Let $\mathbf{u}_2 = \mathscr{H}_{\nu^+}((\mathbf{u}_{\Gamma_2'}^T, \mathbf{0}_{\gamma_*}^T)^T)$ be the discrete ν^+-harmonic extension of $(\mathbf{u}_{\Gamma_2'}^T, \mathbf{0}_{\gamma_*}^T)^T$ into $\tilde{\Omega}_2$, associated with the inner product $a_{\nu^+}(u,v) = \nu^+\int_{\tilde{\Omega}_2}\nabla u\cdot\nabla v\,dx$.
3. Let $\mathbf{u}_*$ be zero extension of $u_*\phi_*$ into Ω_1, where $u_* = u_\Gamma|_{\Gamma_*}$ is the function value of u_Γ at the node Γ_*, and ϕ_* is the basis function at the node Γ_*.

The vector $\mathbf{u}$ is then constructed to be $\mathbf{u} = R_1^T\mathbf{u}_1 + R_2^T\mathbf{u}_2 + \mathbf{u}_*$, where R_1^T is the extension matrix from $\tilde{\Omega}_1$ to Ω_1, and R_2^T is the extension matrix from $\tilde{\Omega}_2$ to Ω_1. Then for any vector norm $\|\cdot\|$, the triangle and Cauchy-Schwarz inequalities give

$$\|\mathbf{u}\|^2 \le \left(\|R_1^T\mathbf{u}_1\| + \|R_2^T\mathbf{u}_2\| + \|\mathbf{u}_*\|\right)^2 \le 3\left(\|R_1^T\mathbf{u}_1\|^2 + \|R_2^T\mathbf{u}_2\|^2 + \|\mathbf{u}_*\|^2\right). \tag{32}$$

We now use the fact that $\tilde{D}^{-1/2}A_\nu\tilde{D}^{-1/2}$ is symmetric positive definite, so that the mapping $\mathbf{v}\mapsto\mathbf{v}^T\tilde{D}^{-1/2}A_\nu\tilde{D}^{-1/2}\mathbf{v}$ defines a norm; therefore, (32) becomes

$$\begin{aligned}\mathbf{u}^T\tilde{D}^{-1/2}A_\nu\tilde{D}^{-1/2}\mathbf{u} &\le 3\Big(\mathbf{u}_1^TR_1\tilde{D}^{-1/2}A_\nu\tilde{D}^{-1/2}R_1^T\mathbf{u}_1\\ &\qquad+\mathbf{u}_2^TR_2\tilde{D}^{-1/2}A_\nu\tilde{D}^{-1/2}R_2^T\mathbf{u}_2+\mathbf{u}_*^T\tilde{D}^{-1/2}A_\nu\tilde{D}^{-1/2}\mathbf{u}_*\Big)\\ &\le 3\left(\mathbf{u}_1^TA_{11}\mathbf{u}_1+\mathbf{u}_2^TA_{22}\mathbf{u}_2+\frac{\nu^-+\nu^+}{2\nu^*}u_*^2A_{\gamma\gamma}\right)\\ &\le 3\left(|u_1|^2_{H^1(\tilde{\Omega}_1)}+|u_2|^2_{H^1(\tilde{\Omega}_2)}+\frac{\nu^-+\nu^+}{2\nu^*}u_*^2|\phi_*|^2_{H^1(\Omega_1)}\right).\end{aligned}$$

By Lemma 6, Lemma 7 and Lemma 3, we know that

1. there exist constants C_1, C_2 and C_3, independent of h, H, ν^- and ν^+, such that
$$|u_1|^2_{H^1(\tilde{\Omega}_1)}\le C_1|u_1|^2_{H^{1/2}(\partial\tilde{\Omega}_1)}\le\frac{C_1C_2}{h}\|u_1\|^2_{L^2(\Gamma_1')}\le C_1C_2C_3\mathbf{u}^T_{\Gamma_1'}\mathbf{u}_{\Gamma_1'}. \tag{33}$$
2. there exist constants C_1', C_2' and C_3', independent of h, H, ν^- and ν^+, such that
$$|u_2|^2_{H^1(\tilde{\Omega}_2)}\le C_1'|u_2|^2_{H^{1/2}(\partial\tilde{\Omega}_2)}\le\frac{C_1'C_2'}{h}\|u_2\|^2_{L^2(\Gamma_2')}\le C_1'C_2'C_3'\mathbf{u}^T_{\Gamma_2'}\mathbf{u}_{\Gamma_2'}. \tag{34}$$
3. By direct calculation, we see that $|\phi_*|^2_{H^1(\Omega_1)}\le C_1''$ for some constant C_1'' independent of h and H.

Combining (31), (33), (34) and the condition for ν^*, we conclude that there exists a constant C, independent of h, H, ν^- and ν^+, such that

$$\mathbf{u}_\Gamma^TD^{-1/2}S_\nu D^{-1/2}\mathbf{u}_\Gamma\le C\mathbf{u}_\Gamma^T\mathbf{u}_\Gamma. \tag{35}$$

This proves the upper bound in (22). The proof of the theorem is therefore completed by noting that the condition number estimate (23) follows immediately from (22). □

Remark 1 We observe from the proof that the lower bound in (22) is actually independent of the choice of ν_*. However, the upper bound does depend on ν_*, so the overall condition number depends on ν_*. This phenomenon can also be observed from the numerical experiments in Table 1 in Section 5.

Proof (Theorem 4) By Theorem 6, the eigenvalues of $Z^{-1}=D^{-1/2}S_\nu D^{-1/2}$ are contained in the interval $[\beta_{\nu,\min},\beta_{\nu,\max}]$, with

$$\beta_{\nu,\min}=\mathscr{O}(h/H)\quad\text{and}\quad\beta_{\nu,\max}=\mathscr{O}(1),$$

respectively. By Theorem 2, we deduce that if we choose the optimal parameter p to follow the asymptotic expression

$$p=p_\nu^*=\frac{\sqrt{\beta_{\nu,\min}\beta_{\nu,\max}}}{h}=\mathscr{O}\left(\frac{1}{\sqrt{Hh}}\right),$$

then the convergence factor is bounded by

$$\rho(M_\nu)\le 1-\sqrt{\beta_{\nu,\min}/\beta_{\nu,\max}}=1-C(h/H)^{1/2},$$

where C is some constant independent of h,H,ν^- and ν^+, as required. □

Remark 2 Theorem 6 indicates that if the Robin parameters are scaled along the artificial interface provided that $\nu^- + \nu^+ < C_* \nu^*$ for some constant C_*, independent of h, H, ν^- and ν^+, then the convergence rate of the discrete zeroth order optimized Schwarz method is independent of the diffusivity. Therefore, we can expect the algorithm to have the same convergence rate as for the constant-coefficient Laplacian. Without this scaling, i.e., if the Robin parameters were the same everywhere, the convergence rate would deteriorate as the heterogeneity ratio ν^+/ν^- increases.

Moreover, Theorem 6 also indicates that the optimal parameter p_ν^* is independent of the heterogeneity, which is of importance in the numerical study. In practice, it is easier for us to find the best parameter p_ν^* on the scale of $1/\sqrt{Hh}$. However, if we use the uniform Robin parameter everywhere, we may have to find the optimal Robin parameter on an extremely small or large scale since $p_1^* = \mathscr{O}(\sqrt{\nu^-\nu^+})\, p_\nu^*$.

4 Analysis for Three Dimensional Problems

Consider the problem

$$\begin{cases} -\nabla\cdot(\nu\nabla u) = 0 & \text{in } \Omega, \\ u = g & \text{on } \bar{\Gamma} = \partial\Omega, \end{cases}$$

where $H > 0$, $\Omega = (-H,H)\times(-H,H)\times(-H,H)$ is decomposed into two non-overlapping subdomains

$$\Omega_1 = (-H,0)\times(-H,H)\times(-H,H), \quad \Omega_2 = (0,H)\times(-H,H)\times(-H,H),$$

and

$$\nu = \begin{cases} \nu^- & \text{in } (-H,H)\times(-H,H)\times(0,H), \\ \nu^+ & \text{in } (-H,H)\times(-H,H)\times(-H,0). \end{cases}$$

Without loss of generality, we still assume that $\nu^+ > \nu^- > 0$.

The analysis for three dimensional problems is similar to that for two dimensional problems, thus we still use A_1 and A_ν to denote the stiffness matrices, L to denote the diagonal matrix containing the Robin parameters, and S_1, S_ν to denote Schur complement matrices after eliminating the interior nodes. The difference is that the matrix $\tilde{A}_\nu$ is now defined by $\tilde{A}_\nu = A_\nu + h^2 L$, since the artificial interface is now a surface. If we mimic the derivation in two dimensions, we obtain

$$\rho(M_\nu) = \rho\left((I-G)(I+G)^{-1}\right),$$

where $G = h^2 \hat{L}^{1/2} S_\nu^{-1} \hat{L}^{1/2}$ and $\hat{L}$ is a positive diagonal matrix. The convergence of the optimized Schwarz method is still guaranteed, so we focus on the two possible choices of the diagonal matrix $\hat{L}$:

(i) $\hat{L} = pI$,
(ii) $\hat{L} = pD = p\cdot\mathrm{diag}(\nu^- I_{n_1}, \nu^* I_{n_*}, \nu^+ I_{n_2})$ with appropriate sizes n_1, n_2 and n_*.

Here we use similar notations to those introduced in Section 3.1, see Figure 4. The difference is that in three dimensions, Γ_* is a line segment from $(0,-H,0)$ to $(0,H,0)$ rather than being a node. Since the matrix G depends on h^2 rather than h, the statement analogous to Theorem 2 is as follows:

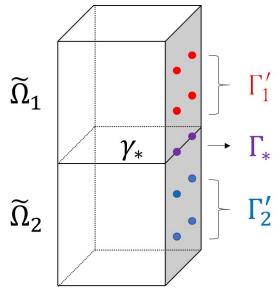

Fig. 4 Notation for different portions of the subdomain and interface for the 3D problem.

Theorem 7 *Let Z be a symmetric positive definite matrix whose eigenvalues are contained in the interval $[\beta_{\min}, \beta_{\max}] \subset (0,\infty)$. Then for $G = h^2 pZ^{-1}$, the choice*

$$p = p^* = \frac{\sqrt{\beta_{\min}\beta_{\max}}}{h^2} \tag{36}$$

leads to the convergence factor

$$\rho(M_\nu) \le 1 - \frac{1-(\beta_{\min}/\beta_{\max})^{1/2}}{1+(\beta_{\min}/\beta_{\max})^{1/2}} \le 1 - \sqrt{\beta_{\min}/\beta_{\max}}, \tag{37}$$

where $M_\nu = (I-G)(I+G)^{-1}$ is the iteration matrix.

Note that the above theorem does not mean that the Robin parameters have a different scaling in the 3D case, since the bounds $\beta_{\min}$ and $\beta_{\max}$ on the Schur complement spectrum will also have a different scaling as a function of h. In fact, the next theorem shows that for the choice $\hat{L} = pI$, i.e., the same Robin parameter everywhere, then the optimal parameter has exactly the same scaling as in the 2D case:

Theorem 8 *For the 3D problem* (4) *with uniform Robin parameter $\hat{L} = pI$, the choice*

$$p = p_1^* = \mathscr{O}\left(\sqrt{\frac{\nu^-\nu^+}{Hh}}\right)$$

leads to the convergence factor

$$\rho\left(M_\nu\right) \le 1 - C\left(\sqrt{\frac{\nu^- h}{\nu^+ H}}\right)$$

for some constant $C > 0$ independent of h, H, ν^- and ν^+.

Proof By an argument that is essentially identical to the one in Theorem 5, we obtain the spectral estimate

$$c\nu^- h^2 H^{-1} \mathbf{u}_\Gamma^T \mathbf{u}_\Gamma \le \mathbf{u}_\Gamma^T S_\nu \mathbf{u}_\Gamma \le Ch\nu^+ \mathbf{u}_\Gamma^T \mathbf{u}_\Gamma, \tag{38}$$

where the only difference with (16) is the scaling in h, due to the problem now being posed in 3D. Hence, the matrix $Z = S_\nu^{-1}$ has eigenvalues lying inside the interval $[\beta_{1,\min}, \beta_{1,\max}]$, where

$$\beta_{1,\min} = \mathscr{O}(\nu^- h^2 H^{-1}) \quad \text{and} \quad \beta_{1,\max} = \mathscr{O}(\nu^+ h),$$

so Theorem 7 says we should choose

$$p_1^* = \frac{\sqrt{\beta_{1,\min}\beta_{1,\max}}}{h^2} = \mathscr{O}\left(\sqrt{\frac{\nu^-\nu^+}{Hh}}\right).$$

The estimate for the convergence rate now follows from (37). □

Our second main result in three dimensions deals with the case of the scaled Robin parameter $\hat{L} = pD = p \cdot \mathrm{diag}(\nu^- I_{n_1}, \nu^* I_{n_*}, \nu^+ I_{n_2})$. Recall that the variables corresponding to ν^* is no longer a single node, but a line separating the upper and the lower parts of the interface, see Figure 4.

Theorem 9 *Let ν^* satisfy $\nu^- + \nu^+ < C_*\nu^*$ for some constant C_*, independent of ν^- and ν^+. Then there exist constants c and C, independent of h, H, ν^- and ν^+, such that*

$$ch^2H^{-1}\mathbf{u}_\Gamma^T\mathbf{u}_\Gamma \le \mathbf{u}_\Gamma^T D^{-1/2}S_\nu D^{-1/2}\mathbf{u}_\Gamma \le Ch\mathbf{u}_\Gamma^T\mathbf{u}_\Gamma. \tag{39}$$

Consequently, there exists a constant C', independent of h, H, ν^- and ν^+, such that

$$\kappa(D^{-1/2}S_\nu D^{-1/2}) < \frac{C'H}{h}. \tag{40}$$

Proof Since $ch^2\mathbf{u}_\Gamma^T\mathbf{u}_\Gamma \le \|u_\Gamma\|^2_{L^2(\Gamma)} \le Ch^2\mathbf{u}_\Gamma^T\mathbf{u}_\Gamma$ (see Lemma 3), we can derive the lower bound by mimicking Theorem 6.

For the upper bound, let $\mathbf{u}_1 = \mathscr{H}_{\nu^-}((\mathbf{u}_{\Gamma_1'}^T, \mathbf{0}_{\gamma_*}^T)^T)$ be the discrete ν^--harmonic extension of $(\mathbf{u}_{\Gamma_1'}^T, \mathbf{0}_{\gamma_*}^T)^T$ into $\tilde{\Omega}_1$, let $\mathbf{u}_2 = \mathscr{H}_{\nu^+}((\mathbf{u}_{\Gamma_2'}^T, \mathbf{0}_{\gamma_*}^T)^T)$ be the discrete ν^+-harmonic extension of $(\mathbf{u}_{\Gamma_2'}^T, \mathbf{0}_{\gamma_*}^T)^T$ into $\tilde{\Omega}_2$, and let $\mathbf{u}_*$ be the zero extension of $\sum_{x_*\in\Gamma_*} u_*(x_*)\phi_*(x_*)$ into Ω_1, where x_* is a node on Γ_*, $u_*(x_*) = u_\Gamma|_{x_*}$ and $\phi_*(x_*)$ is the basis function at x_*. We construct $\mathbf{u} = R_1^T\mathbf{u}_1 + R_2^T\mathbf{u}_2 + \mathbf{u}_*$, where R_1^T is the extension matrix from $\tilde{\Omega}_1$ to Ω_1, and R_2^T is the extension matrix from $\tilde{\Omega}_2$ to Ω_1. Then we have

$$\begin{aligned}
\mathbf{u}_\Gamma^T D^{-1/2}S_\nu D^{-1/2}\mathbf{u}_\Gamma &\le \mathbf{u}^T\tilde{D}^{-1/2}A_\nu\tilde{D}^{-1/2}\mathbf{u} \\
&\le 3\left(|u_1|^2_{H^1(\tilde{\Omega}_1)} + |u_2|^2_{H^1(\tilde{\Omega}_2)} + \frac{1}{2}C_*\mathbf{u}_*^T A_{\gamma\gamma}\mathbf{u}_*\right) \\
&\le C_1|u_1|^2_{H^{1/2}(\partial\tilde{\Omega}_1)} + C_1'|u_2|^2_{H^{1/2}(\partial\tilde{\Omega}_2)} + \frac{3}{2}C_*\mathbf{u}_*^T A_{\gamma\gamma}\mathbf{u}_* \\
&\le \frac{C_1C_2}{h}\|u_1\|^2_{L^2(\Gamma_1)} + \frac{C_1'C_2'}{h}\|u_2\|^2_{L^2(\Gamma_2)} + \frac{3}{2}C_*\mathbf{u}_*^T A_{\gamma\gamma}\mathbf{u}_* \\
&\le C_1C_2C_3h\,\mathbf{u}_1^T\mathbf{u}_1 + C_1'C_2'C_3'h\,\mathbf{u}_2^T\mathbf{u}_2 + \frac{3}{2}C_*\mathbf{u}_*^T A_{\gamma\gamma}\mathbf{u}_*,
\end{aligned} \tag{41}$$

where we have mimicked Theorem 6 for the second inequality, and we have used Lemma 6, Lemma 7 and Lemma 3 at the third, the fourth and the fifth inequality, respectively.

We now estimate the term $\mathbf{u}_*^T A_{\gamma\gamma}\mathbf{u}_*$ as follows. Since all the nodes on Γ_* lie on a line, we can order them contiguously as $x_1, \ldots, x_N$, so that x_i and x_j are neighbours whenever $|i-j| = 1$. By doing so, we see that for any non-neighbouring nodes i and j, the supports of their nodal basis functions do not overlap, so we have

$$a_1(\phi_i, \phi_j) = \int_{\Omega_1} \nabla\phi_i \cdot \nabla\phi_j\, dx = 0 \qquad \text{whenever} |i-j| \ge 2.$$

For $|i-j| \leq 1$, we have by direct calculation $a_1(\phi_i, \phi_j) \leq C_1'' h$. Therefore, defining for notational convenience the two ghost values $u_*(x_0) = u_*(x_{N+1}) = 0$, we have

$$\begin{aligned}
\mathbf{u}_*'^T A_{\gamma\gamma} \mathbf{u}_*' &= \sum_{i=1}^{N} \sum_{j=1}^{N} a(\phi_i, \phi_j) u_*(x_i) u_*(x_j) \\
&\leq C_1'' h \sum_{i=1}^{N} \left(\left|u_*(x_{i-1})\right| \left|u_*(x_i)\right| + \left|u_*(x_i)\right|^2 + \left|u_*(x_i)\right| \left|u_*(x_{i+1})\right| \right) \\
&\leq 3 C_1'' h \sum_{i=1}^{N} \left|u_*(x_i)\right|^2 \\
&= 3 C_1'' h \mathbf{u}_*'^T \mathbf{u}_*'.
\end{aligned} \tag{42}$$

Combining (41) and (42), we have for some constant C, independent of h, H, ν^- and ν^+ such that

$$\mathbf{u}_\Gamma^T D^{-1/2} S_\nu D^{-1/2} \mathbf{u}_\Gamma \leq Ch \mathbf{u}_\Gamma^T \mathbf{u}_\Gamma.$$

Now we have proved (39), from which we obtain (40). □

The above theorem implies that the matrix $Z = D^{-1/2} S_\nu D^{-1/2}$ has eigenvalues within the interval $[ch^2 H^{-1}, Ch]$. Theorem 7 can now be used to determine the optimal parameter p and the resulting convergence rate.

Theorem 10 *Consider the 3D problem* (4) *with the scaled Robin parameters*

$$\hat{L} = p \cdot \mathrm{diag}(\nu^- I_{n_1}, \nu^* I_{n_*}, \nu^+ I_{n_2}),$$

where n_1, n_2 and n_* are the number of degrees of freedom in Γ_1', Γ_2' and Γ_* respectively, see Figure 4. Then the choice

$$p = p_\nu^* = \mathscr{O}\left(\frac{1}{\sqrt{Hh}}\right) \tag{43}$$

leads to the convergence factor

$$\rho(M_\nu) \leq 1 - C\sqrt{\frac{h}{H}}, \tag{44}$$

with the constant C independent of h, H, ν^- and ν^+.

5 Numerical Experiments

In this section, we will illustrate our theoretical results by applying the optimized Schwarz method to some numerical examples. In particular, we will also consider examples where the analysis assumptions do not hold, in order to see whether our recommended Robin parameters would make a good heuristic choice in more general cases. We will show numerical results for the optimized Schwarz method both when used as a stationary method, and when used as a preconditioner for GMRES.

For each test below, we generate a random initial guess between -1 and 1 so that the initial error contains as many frequencies as possible. We discretize the problem using the P^1 finite element method and solve the resulting system with a tolerance TOL $< 10^{-6}$ for both stationary iteration and GMRES method.

Test 1: Model Problem

In the first set of tests, we consider our model problem

$$\begin{cases} -\nabla\cdot(\nu\nabla u) = 0 & \text{in } \Omega = (-\frac{\pi}{2},\frac{\pi}{2})\times(-\frac{\pi}{2},\frac{\pi}{2}), \\ u = 0 & \text{on } \partial\Omega, \end{cases} \tag{45}$$

where

$$\nu = \begin{cases} \nu_1 & \text{in } (-\frac{\pi}{2},\frac{\pi}{2})\times(0,\frac{\pi}{2}), \\ \nu_2 & \text{in } (-\frac{\pi}{2},\frac{\pi}{2})\times(-\frac{\pi}{2},0). \end{cases}$$

The domain is decomposed into two nonoverlapping subdomains $\Omega_1 = (-\frac{\pi}{2},0)\times(-\frac{\pi}{2},\frac{\pi}{2})$ and $\Omega_2 = (0,\frac{\pi}{2})\times(-\frac{\pi}{2},\frac{\pi}{2})$.

First of all, we look at the eigenvalues of the Schur complement matrix S_ν with $\nu_1 = 1$ and $H = \pi$. We discretize the problem by the P^1 finite element method and construct S_ν and $D^{-1/2}S_\nu D^{-1/2}$ by eliminating the interior nodes. We report the minimum and maximum eigenvalues in Table 1. We can observe that the numerical results match the theory, especially in the following aspects:

1. For the smallest and the largest eigenvalues of S_ν, i.e., $\beta_{1,\min}$ and $\beta_{1,\max}$, we have $\beta_{1,\min} = \mathscr{O}(h)$ and $\beta_{1,\max} = \mathscr{O}(\nu_2)$. Numerical results match both estimates well since we can see that for a fixed heterogeneity ratio, the smallest eigenvalue $\beta_{1,\min}$ decreases linearly as we refine the mesh, while the largest eigenvalue $\beta_{1,\max}$ is independent of the mesh size; for a fixed mesh size, the largest eigenvalues increase as we enlarge the heterogeneity ratio.
2. For the smallest and largest eigenvalues of $D^{-1/2}S_\nu D^{-1/2}$, i.e., $\beta_{\nu,\min}$ and $\beta_{\nu,\max}$, we have $\beta_{\nu,\min} = \mathscr{O}(h)$ and $\beta_{\nu,\max} = \mathscr{O}(1)$, provided $\nu_1 + \nu_2 < C_*\nu^*$ for some constant C_* independent of ν_1 and ν_2. To choose such ν^*, intuitively we have two choices: $\nu^* = \frac{\nu_1+\nu_2}{2}$ or $\nu^* = \nu_2$. We report the results for both two choices. We can observe from the table that the preconditioners are very robust as long as ν^* is chosen to be one of these two numbers, and the corresponding numerical results perfectly match the theory. We also list the results when $\nu^* = \nu_1$. In that case, the condition for ν^* is not satisfied. As a result, the robustness of this preconditioner is deteriorated.

Next, we show the convergence results of OSM applied to the model problem. We refer to (10) to find the best Robin parameter when it is uniform along the artificial interface, and to (12) to find the scaled parameter.

Recall that we have two ways of computing the integral along the interface in the weak form (3). One way is to use the lumped numerical integration, from which we can obtain the diagonal matrix discussed in this paper. The other way is to use consistent integration (i.e., exact integration), which yields a tri-diagonal matrix. We test (45) by OSM with the scaled Robin parameter, with or without lumped integration along the interface, and report the results in Table 2. We can observe that OSM with the lumped integration converges faster than that without lumped integration. This is consistent with the discussion in [13]. In the remaining tests, we will use the lumped integration.

In Table 3, we report the linear iteration counts needed by OSM with and without Krylov acceleration for (45). For each mesh size, we also compare the results of OSM with the scaled Robin parameter and with the uniform one. We can see that the results for the scaled

Table 1 The smallest and the largest eigenvalues of S_ν and $D^{-1/2}S_\nu D^{-1/2}$ with different mesh sizes, ν^* and heterogeneity ratios.

h	ν_1/ν_2	$\beta_{1,\min}$	$\beta_{1,\max}$	ν^*	$\beta_{\nu,\min}$	$\beta_{\nu,\max}$
$\frac{\pi}{20}$	1/10	0.2735	2.7881e+01	ν_1	0.1671	9.5691
				$(\nu_1+\nu_2)/2$	0.1560	2.8176
				ν_2	0.1441	2.7885
	1/100	0.2872	2.7879e+02	ν_1	0.1691	8.3267e+01
				$(\nu_1+\nu_2)/2$	0.1560	2.8176
				ν_2	0.1416	2.7879
	1/1000	0.2885	2.7879e+03	ν_1	0.1693	8.2076e+02
				$(\nu_1+\nu_2)/2$	0.1560	2.8176
				ν_2	0.1414	2.7879
$\frac{\pi}{40}$	1/10	0.1425	2.8170e+01	ν_1	0.0847	9.5633
				$(\nu_1+\nu_2)/2$	0.0816	2.8255
				ν_2	0.0783	2.8170
	1/100	0.1497	2.8169e+02	ν_1	0.0852	8.3187e+01
				$(\nu_1+\nu_2)/2$	0.0816	2.8255
				ν_2	0.0776	2.8169
	1/1000	0.1504	2.8169e+03	ν_1	0.0853	8.1994e+02
				$(\nu_1+\nu_2)/2$	0.0816	2.8255
				ν_2	0.0776	2.8169
$\frac{\pi}{80}$	1/10	0.0729	2.8254e+01	ν_1	0.0426	9.5617
				$(\nu_1+\nu_2)/2$	0.0418	2.8276
				ν_2	0.0409	2.8254
	1/100	0.0766	2.8254e+02	ν_1	0.0427	8.3165e+01
				$(\nu_1+\nu_2)/2$	0.0418	2.8276
				ν_2	0.0407	2.8254
	1/1000	0.0769	2.8254e+03	ν_1	0.0428	8.1971e+02
				$(\nu_1+\nu_2)/2$	0.0418	2.8276
				ν_2	0.0407	2.8254

Table 2 The number of linear iterations needed by OSM with the scaled Robin parameter for the model problem.

Optimized Schwarz method as an iterative method					
h	With Lumping \ ν_1/ν_2	1/10	1/100	1/1000	1/10000
$\frac{\pi}{20}$	No	39	69	73	74
	Yes	31	31	31	31
$\frac{\pi}{40}$	No	51	52	63	64
	Yes	44	44	44	44
$\frac{\pi}{80}$	No	65	81	82	82
	Yes	63	63	63	63

Robin parameter are better than those for the uniform Robin parameter. In addition, the number of linear iterations remains unchanged as we increase the heterogeneity ratio when we use the scaled Robin parameter. In contrast, the iteration count grows proportionally to the square root of the heterogeneity ratio when we use the uniform Robin parameter, thereby illustrating the deterioration of the convergence factor. When a Krylov method is applied, we can observe great improvements in terms of the number of linear iterations needed by two versions. But we can still see that the results for the scaled Robin parameter outperforms those for the uniform one. Besides, we observe that the linear iteration counts needed by Krylov accelerated OSM with the scaled Robin parameter remains approximately

Table 3 The number of linear iterations needed by OSM with the scaled or the uniform Robin parameters for the model problem.

Optimized Schwarz method as an iterative method					
OSM Version	H/h \ ν_1/ν_2	1/10	1/100	1/1000	1/10000
uniform p	20	71	225	713	2256
	40	105	334	1059	3348
	80	147	464	1470	4648
scaled p	20	31	31	31	31
	40	44	44	44	44
	80	63	63	63	63
Optimized Schwarz method with Krylov acceleration					
uniform p	20	22	30	31	31
	40	28	40	47	48
	80	34	52	65	66
scaled p	20	14	15	15	15
	40	18	18	18	18
	80	22	22	22	22

unchanged when the heterogeneity ratio increases, whereas the number needed by Krylov accelerated OSM with the uniform Robin parameter grows with the heterogeneity ratio.

Test 2: Problem with Multiple Diffusivity Regions

In the second set of tests, we consider the problem

$$\begin{cases} -\nabla\cdot(\nu\nabla u) = 0 & \text{in } \Omega = (-\frac{\pi}{2},\frac{\pi}{2})\times(-\frac{\pi}{2},\frac{\pi}{2}), \\ u = 0 & \text{on } \partial\Omega, \end{cases} \tag{46}$$

where we now increase the number of discontinuities:

$$\nu = \begin{cases} \nu_1 & \text{in } (-\frac{\pi}{2},\frac{\pi}{2})\times(\frac{\pi}{4},\frac{\pi}{2}), \\ \nu_2 & \text{in } (-\frac{\pi}{2},\frac{\pi}{2})\times(0,\frac{\pi}{4}), \\ \nu_3 & \text{in } (-\frac{\pi}{2},\frac{\pi}{2})\times(-\frac{\pi}{4},0), \\ \nu_4 & \text{in } (-\frac{\pi}{2},\frac{\pi}{2})\times(-\frac{\pi}{2},-\frac{\pi}{4}). \end{cases}$$

In this set of tests, we let $\nu_1 = 1$, $\nu_2 = 10$, $\nu_3 = 1000$ and $\nu_4 = 50$. In comparison test, we change the order of the diffusivity, letting $\nu_1 = 1$, $\nu_2 = 1000$, $\nu_3 = 50$ and $\nu_4 = 10$. Moreover, we will decompose the domain Ω into either $N = 2$ and $N = 4$ subdomains consisting of vertical strips of equal width. In other words, we have $\Omega_i = I_i \times (-\pi/2, \pi/2)$ with $I_1 = (-\pi/2, 0)$, $I_2 = (0, \pi/2)$ for $N = 2$, and $I_1 = (-\pi/2, -\pi/4)$, $I_2 = (-\pi/4, 0)$, etc. for $N = 4$.

We can see in Table 4 that results for the scaled Robin parameter always outperforms those for the uniform one, requiring much fewer linear iterations to converge. Besides, we can observe for both $N = 2$ and $N = 4$ that the convergence of OSM with the scaled Robin parameter is independent of the heterogeneity ratio, whereas the convergence of the uniform one depends on the smallest and the largest diffusion coefficients, no matter how these coefficients are ordered.

Table 4 The number of linear iterations needed by OSM with the scaled or the uniform Robin parameter for the problem with four diffusivity regions and $N = 2$ or 4 subdomains.

Optimized Schwarz method as an iterative method					
OSM Version	$\nu_1/\nu_2/\nu_3/\nu_4$ / H/h	$N=2$		$N=4$	
		1/10/1000/50	1/1000/50/10	1/10/1000/50	1/1000/50/10
uniform p	20	442	424	475	434
	40	595	590	652	648
	80	870	843	925	877
scaled p	20	37	37	40	39
	40	50	53	60	58
	80	71	72	81	84
Optimized Schwarz method with Krylov acceleration					
uniform p	20	36	36	57	56
	40	57	54	72	71
	80	74	76	85	84
scaled p	20	15	15	19	19
	40	18	18	23	23
	80	22	22	28	28

Test 3: Three-Dimensional Problem

In the third set of tests, we study the numerical behavior of the optimized Schwarz method for the following three dimensional problem

$$\begin{cases} -\nabla\cdot(\nu\nabla u) = 0 & \text{in } \Omega = (-\frac{\pi}{2},\frac{\pi}{2})\times(-\frac{\pi}{2},\frac{\pi}{2})\times(-\frac{\pi}{2},\frac{\pi}{2}), \\ u = 0 & \text{on } \partial\Omega, \end{cases} \tag{47}$$

where

$$\nu = \begin{cases} \nu_1 & \text{in } (-\frac{\pi}{2},\frac{\pi}{2})\times(-\frac{\pi}{2},\frac{\pi}{2})\times(0,\frac{\pi}{2}), \\ \nu_2 & \text{in } (-\frac{\pi}{2},\frac{\pi}{2})\times(-\frac{\pi}{2},\frac{\pi}{2})\times(-\frac{\pi}{2},0), \end{cases}$$

The domain is decomposed into two nonoverlapping subdomains $\Omega_1 = (-\frac{\pi}{2},0)\times(-\frac{\pi}{2},\frac{\pi}{2})\times(-\frac{\pi}{2},\frac{\pi}{2})$ and $\Omega_2 = (0,\frac{\pi}{2})\times(-\frac{\pi}{2},\frac{\pi}{2})\times(-\frac{\pi}{2},\frac{\pi}{2})$.

The numerical results are shown in Table 5. We observe that the convergence of OSM with the scaled Robin parameter only depends on the mesh size h, requiring for each mesh size much fewer linear iterations than OSM with the uniform Robin parameter.

Test 4: Problem with Unstructured Mesh

In the fourth set of tests, we will show the results when the mesh is unstructured, so that the subdomain boundary does not cut perpendicularly to the discontinuity.

The problem we consider in this set of tests is

$$\begin{cases} -\nabla\cdot(\nu\nabla u) = 0 & \text{in } \Omega = (-\frac{\pi}{2},\frac{\pi}{2})\times(-\frac{\pi}{2},\frac{\pi}{2}), \\ u = 0 & \text{on } \partial\Omega, \end{cases} \tag{48}$$

Table 5 The number of linear iterations needed by OSM with the scaled or the uniform Robin parameter for the three-dimensional problem.

Optimized Schwarz method as an iterative method					
OSM Version	H/h \ ν_1/ν_2	1/10	1/100	1/1000	1/10000
uniform p	10	59	189	600	1897
	20	86	274	868	2745
	40	124	393	1245	3932
scaled p	20	20	20	20	20
	40	27	27	27	27
	80	41	41	41	41
Optimized Schwarz method with Krylov acceleration					
uniform p	10	23	33	37	36
	20	29	46	55	56
	40	36	58	74	78
scaled p	10	13	13	13	13
	20	17	18	18	18
	40	22	22	22	22

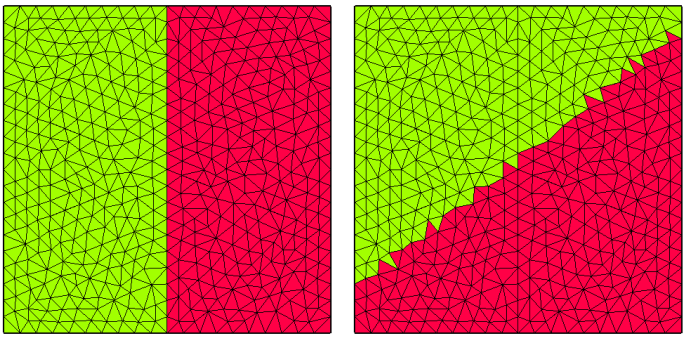

Fig. 5 Heterogeneity and domain decomposition for Test 4.

with the heterogeneity defined by

$$\nu = \begin{cases} \nu_1, & x < 0, \\ \nu_2, & x > 0, \end{cases}$$

We construct an unstructured mesh with approximately 20 degrees of freedom in each direction. We cut the domain into two nonoverlapping subdomains approximately along $y = 0.8x + 0.1$. We show in Figure 5 the heterogeneity and the domain decomposition.

In Table 6, we show a comparison of two versions of OSM. Again we see the perfect convergence behavior of OSM with the scaled Robin parameter, whereas the convergence of OSM with the uniform Robin parameter deteriorates as we increase the heterogeneity ratio.

Table 6 Linear counts needed by OSM with scaled or uniform Robin parameters for the problem with an unstructured mesh. The tolerance is set to be 10^{-6}.

Optimized Schwarz method as an iterative method					
OSM Version	H/h \ ν_1/ν_2	1/10	1/100	1/1000	1/10000
uniform p	20	99	312	989	3134
	40	116	377	1205	3822
	80	183	563	1782	5642
scaled p	20	36	37	37	40
	40	55	57	59	59
	80	76	77	78	76
Optimized Schwarz method with Krylov acceleration					
uniform p	20	27	38	41	41
	40	33	47	54	54
	80	40	61	75	78
scaled p	20	21	21	21	21
	40	24	24	24	24
	80	28	29	29	29

Test 5: Problem with Oscillatory Diffusivity

We now consider the problem

$$\begin{cases} -\nabla\cdot(\nu(x,y)\nabla u) = 0 & \text{in } \Omega = (-\frac{\pi}{2},\frac{\pi}{2})\times(-\frac{\pi}{2},\frac{\pi}{2}), \\ u = 0 & \text{on } \partial\Omega, \end{cases} \tag{49}$$

with $\nu(x,y)$ being defined by

$$\nu(x,y) = (\nu_2-\nu_1)\cos^2(5(x+y-1))+\nu_1,$$

where ν_1 and ν_2 are two positive constants. Note that the diffusion coefficient oscillates over the whole domain. We cut the domain into two nonoverlapping subdomains $\Omega_1 = (-\frac{\pi}{2},0)\times(-\frac{\pi}{2},\frac{\pi}{2})$ and $\Omega_2 = (0,\frac{\pi}{2})\times(-\frac{\pi}{2},\frac{\pi}{2})$. In that case, at each grid point on the artificial interface, the Robin parameter needs to be chosen carefully in order to satisfy the condition for ν^* in Theorem 6. To implement this, at each point on the interface, we choose the largest among the function value at this node and those at the neighboring nodes. We also show in Figure 6 a plot of the diffusivity, the domain decomposition and the mesh. The number of linear iterations is reported in Table 7. We observe that the convergence of OSM with the scaled Robin parameter is much faster than that of OSM with the uniform Robin parameter for both the iterative and Krylov methods. However, when the optimized Schwarz method is treated as an iterative method, the number of linear iterations also grows slightly as we increase the heterogeneity ratio. The reason is that this choice of the scaled Robin parameter only depends on the nodal diffusivity. In general, the maximum of the diffusivity is not located at any of these nodes, so that there is a possibility that the average on a finite element boundary on the artificial interface is larger than the Robin parameter we use for Table 7. As a result, such nodally scaled Robin parameter may not satisfy the condition for ν^* in Theorem 6.

To fix the problem, we introduce a smoothly scaled Robin parameter for the current test. On each finite element edge Γ_e on the artificial interface, we compute the average by

$$\bar{\nu}_{\Gamma_e} = \frac{1}{|\Gamma_e|}\int_{\Gamma_e}\nu(x,y)\,dx. \tag{50}$$

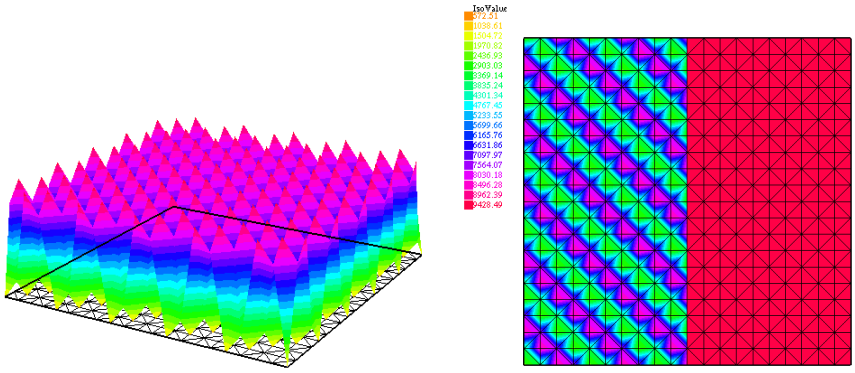

Fig. 6 Left: diffusion coefficient in test 5 with $\nu_1 = 1$ and $\nu_2 = 10$. Right: 2D plot of the coefficient, the left subdomain and the mesh with $h = \frac{1}{20}$ on the left, glued to the right subdomain and the mesh on the right.

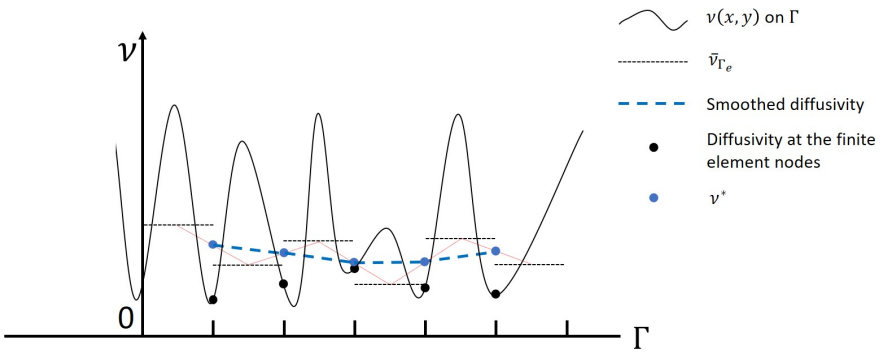

Fig. 7 Construction of smoothly scaled Robin parameters for oscillatory diffusivity.

The resulting piecewise constant (i.e., P^0) finite element function on the artificial interface is then interpolated linearly to a P^1 finite element function. Note that this function can be regarded as a smoothed expression of the diffusion coefficient. The smoothly scaled Robin parameter is then chosen to be proportional to this smoothed diffusion coefficient, see Figure 7. We report the data in Table 8 where we compare the results for the smoothly scaled Robin parameter with those for the nodally scaled Robin parameter (in bracket). We can see that the results for the smoothly scaled Robin parameter are improved, and the number of linear iterations remains almost unchanged when the optimized Schwarz method is treated as an iterative solver.

Table 7 Linear counts needed by with scaled or uniform Robin parameters for the problem with oscillatory diffusivity. The tolerance is set to be 10^{-6}.

Optimized Schwarz method as an iterative method					
OSM Version	H/h \ ν_1/ν_2	1/10	1/100	1/1000	1/10000
uniform p	20	36	71	225	731
	40	60	187	593	1873
	80	97	306	970	3066
scaled p	20	31	36	37	37
	40	46	51	52	52
	80	72	77	83	84
Optimized Schwarz method with Krylov acceleration					
uniform p	20	16	23	26	27
	40	23	31	41	45
	80	29	51	73	80
scaled p	20	15	16	16	16
	40	21	22	23	23
	80	21	28	28	28

Table 8 The number of linear counts needed by OSM with the smoothly scaled or the nodally scaled (in brackets) Robin parameter for the problem with oscillatory diffusivity.

Optimized Schwarz method as an iterative method				
H/h \ ν_1/ν_2	1/10	1/100	1/1000	1/10000
20	28(31)	29(36)	29(37)	29(37)
40	43(46)	45(51)	46(52)	46(52)
80	71(72)	71(77)	73(83)	73(84)
Optimized Schwarz method with Krylov acceleration				
20	15(15)	15(16)	15(16)	15(16)
40	20(21)	20(22)	21(23)	21(23)
80	25(27)	26(28)	27(28)	27(28)

Test 6: Problem with a cross point

Finally, we consider the problem of four subdomains meeting at a single coarse point. More precisely, we consider the problem

$$\begin{cases} -\nabla\cdot(\nu(x,y)\nabla u) = 0 & \text{in } \Omega = (-\frac{\pi}{2},\frac{\pi}{2})\times(-\frac{\pi}{2},\frac{\pi}{2}), \\ u = 0 & \text{on } \partial\Omega, \end{cases} \tag{51}$$

with

$$\nu(x,y) = \begin{cases} \nu_1, & y\in(-\frac{\pi}{4},0)\cup(\frac{\pi}{4},\frac{\pi}{2}), \\ \nu_2, & y\in(-\frac{\pi}{2},-\frac{\pi}{4})\cup(0,\frac{\pi}{4}). \end{cases}$$

The four subdomains correspond to the part of the square within each quadrant, see Figure 8. In this configuration, each subdomain contains two subregions with different diffusivities. Long the interfaces Γ_{12} and Γ_{34}, the diffusivity is discontinuous along the interface; we therefore test our two choices of Robin parameter p, with either a constant parameter or a scaling proportional to the local diffusivity. Along Γ_{23} and Γ_{14}, the interface is aligned with the discontinuity in the diffusivity; we therefore follow [10] and choose p to be proportional

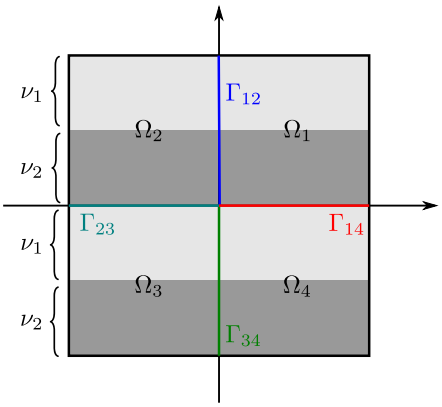

Fig. 8 Test case with four subdomains meeting at a cross point at the origin.

Table 9 The number of linear counts needed by OSM with the scaled or the uniform Robin parameter for the decomposition with a cross point and with non-conforming heterogeneities.

Optimized Schwarz method as an iterative method					
OSM Version	H/h \ ν_1/ν_2	1/10	1/100	1/1000	1/10000
uniform p	20	44	133	422	1334
	40	66	206	654	2068
	80	174	316	999	3160
scaled p	20	25	25	25	25
	40	36	36	36	36
	80	49	49	49	49
Optimized Schwarz method with Krylov acceleration					
uniform p	20	23	36	38	39
	40	28	48	59	63
	80	37	63	89	97
scaled p	20	14	13	13	13
	40	17	16	16	16
	80	21	20	20	20

to the diffusivity of the *neighbouring* subdomain, e.g., for the subdomain Ω_1, we impose

$$\left(\nu_2 \frac{\partial}{\partial \mathbf{n}_1} + p^* \nu_1\right) u_1^{n+1} = \left(\nu_2 \frac{\partial}{\partial \mathbf{n}_1} + p^* \nu_1\right) u_4^n \qquad \text{on } \Gamma_{14}$$

with $p^* \approx 2.8/\sqrt{h}$. The Robin parameter p_0 at the origin is taken to be $p_0 = \frac{C}{\sqrt{h}} \cdot \frac{\nu_1+\nu_2}{2}$, with the best C determined numerically to be 0.42. The convergence of the resulting algorithm is shown in Table 9. Just as in the other test cases, scaling the Robin parameter along non-conforming interfaces leads to much lower iteration counts and a robust convergence behaviour with respect to the heterogeneity ratio, which is not the case when a uniform Robin parameter is used instead.

6 Conclusions

In this paper, we have studied the zeroth order optimized Schwarz method for domains with non-conforming heterogeneities. We have shown that the zeroth order optimized Schwarz method with traditional uniform Robin parameter is not robust any more for highly heterogeneous problems. To overcome this difficulty, we propose a scaled Robin parameter which is proportional to the diffusivity. The optimal Robin parameter is easy to find, and the resulting convergence rate is independent of the diffusivity. We have also tested several problems in two and three dimensions numerically using our method. The method is shown to work very well for all tests.

Acknowledgment. We thank the anonymous referee for their helpful comments, which led to a significant improvement in the quality of the paper. A portion of this research was conducted while the authors were at Hong Kong Baptist University.

Funding. This work is partially supported by the NSERC Discovery Grant (Canada, Ref. No. RGPIN-2021-02595), the Research Grants Council of the Hong Kong SAR, China (Project No. HKBU 12301817, HKBU 12301018) and the National Natural Science Foundation of China (Young Scientist Fund No. 11501483).

Data Availability Statement. Data sharing is not applicable to this article as no datasets were generated or analysed during the current study.

A Useful Sobolev-type estimates

Lemma 3 ([28], Lemma B.5) *Let ϕ be a basis function associated with a node of an element $K \subset \Omega \subset \mathbb{R}^n$, Then there exist constants c and C, independent of h, such that*

$$ch^n \le \|\phi\|^2_{L^2(K)} \le Ch^n.$$

Consequently, for any u_Γ, the trace of a finite element function on Γ, there exist constants c_1 and C_1, independent of h and H, such that

$$c_1 h^{n-1} \mathbf{u}_\Gamma^T \mathbf{u}_\Gamma \le \|u_\Gamma\|^2_{L^2(\Gamma)} \le C_1 h^{n-1} \mathbf{u}_\Gamma^T \mathbf{u}_\Gamma.$$

Lemma 4 ([28], Lemma A.14 and Corollary A.15) *Let Ω be a Lipschitz continuous domain with diameter H. Let $\Gamma \in \partial\Omega$ have nonvanishing measure. If $u \in H^1(\Omega)$ vanishes on Γ, then there exists a constant C, independent of H, such that*

$$\|u\|^2_{L^2(\Omega)} \le C^2 H^2 |u|^2_{H^1(\Omega)}.$$

Moreover, if we define

$$\|u\|^2_{H^1_s(\Omega)} := |u|^2_{H^1(\Omega)} + \frac{1}{H^2}\|u\|^2_{L^2(\Omega)}$$

as the scaled H^1-norm, then we obtain the following estimate:

$$\|u\|^2_{H^1_s(\Omega)} \le (1+C^2)|u|^2_{H^1(\Omega)}.$$

Lemma 5 *Let u_Γ be the trace of a finite element function on Γ, and let $\mathbf{u}_\Gamma$ be the vector corresponding to u_Γ. Let A_1 be the stiffness matrix associated with the standard Laplacian bilinear form, and S_1 be its Schur complement after the interior nodes have been eliminated. Then there exist constants c and C, independent of h and H, such that the following sharp estimate holds:*

$$cH^{-1}\|u_\Gamma\|^2_{L^2(\Gamma)} \le \mathbf{u}_\Gamma^T S_1 \mathbf{u}_\Gamma \le Ch^{-1}\|u_\Gamma\|^2_{L^2(\Gamma)}, \tag{52}$$

where h is the diameter of the finite element, and H is the diameter of the subdomain. Consequently, there exists a constant C', independent of h and H, such that

$$\kappa(S_1) < C' \frac{H}{h}. \tag{53}$$

Proof The proof is based on Lemma 4.11 in [28], where the authors have derived the upper bound. For the lower bound, they have also proved that

$$H\|u\|^2_{L^2(\Gamma)} \leq H^2\|u\|^2_{H^{1/2}(\Gamma)} \leq C_t^2 \left(H^2|u|^2_{H^1(\Omega_i)} + \|u\|^2_{L^2(\Omega_i)} \right),$$

where C_t is a constant independent of h and H. Simplification of the above inequality gives

$$H^{-1}\|u\|^2_{L^2(\Gamma)} \leq C_t^2 \left(|u|^2_{H^1(\Omega_i)} + \frac{1}{H^2}\|u\|^2_{L^2(\Omega_i)} \right) = C_t^2 \|u\|^2_{H^1_s(\Omega_i)},$$

where we have used the definition of the scaled H^1-norm (see also (4.4) in [28]). By Lemma 4, we obtain

$$H^{-1}\|u\|^2_{L^2(\Gamma)} \leq C|u|^2_{H^1(\Omega_i)}. \tag{54}$$

Since $\mathbf{u}_\Gamma^T S_1 \mathbf{u}_\Gamma = |u|^2_{H^1(\Omega_i)}$, actually we have finished the proof for the lower bound.

The condition number estimate is then a direct result from the spectral estimates. Note that $\kappa(S_1)$ is none other than the condition number of the Schur complement matrix for the Laplace operator. □

Lemma 6 ([28], Lemma 4.10) *Let Ω be a domain, and let a finite element trace function u_Γ be given on the boundary $\Gamma = \partial\Omega$. Let $\mathbf{u} = \mathscr{H}_1(\mathbf{u}_\Gamma)$ be the discrete 1-harmonic extension of u_Γ into Ω. Then there exist constants c and C, independent of h and H, such that*

$$c\,|u_\Gamma|^2_{H^{1/2}(\Gamma)} \leq |u|^2_{H^1(\Omega_1)} \leq C\,|u_\Gamma|^2_{H^{1/2}(\Gamma)}. \tag{55}$$

Lemma 7 ([11], Lemma 4.5) *Let Ω be a domain, and let a finite element trace function u_Γ be given on the boundary $\Gamma = \partial\Omega$. Then there exist a constant C, independent of h and H, such that*

$$|u_\Gamma|^2_{H^{1/2}(\Gamma)} \leq \frac{C}{h}\|u_\Gamma\|^2_{L^2(\Gamma)}. \tag{56}$$

Lemma 8 ([28], Lemma A.17) *Let Ω be a bounded Lipschitz continuous polygon or polyhedron with diameter H. Then for any $u \in H^{1/2}(\partial\Omega)$ such that the measure of the set $\{x \in \partial\Omega; u(x) = 0.\}$ is non-zero, there exists a constant C, independent of h, such that*

$$\|u\|^2_{L^2(\partial\Omega)} \leq CH|u|^2_{H^{1/2}(\partial\Omega)}. \tag{57}$$

References

1. Bennequin, D., Gander, M., Halpern, L.: A homographic best approximation problem with application to optimized Schwarz waveform relaxation. Mathematics of Computation **78**(265), 185–223 (2009)
2. Berninger, H., Kornhuber, R., Sander, O.: Convergence behaviour of Dirichlet–Neumann and Robin methods for a nonlinear transmission problem. In: Domain decomposition methods in science and engineering XIX, pp. 87–98. Springer (2011)
3. Berninger, H., Loisel, S., Sander, O.: The 2-Lagrange multiplier method applied to nonlinear transmission problems for the Richards equation in heterogeneous soil with cross points. SIAM Journal on Scientific Computing **36**(5), A2166–A2198 (2014)
4. Caetano, F., Gander, M.J., Halpern, L., Szeftel, J.: Schwarz waveform relaxation algorithms with nonlinear transmission conditions for reaction-diffusion equations. In: Domain decomposition methods in science and engineering XIX, pp. 245–252. Springer (2011)
5. Christie, M.A., Blunt, M., et al.: Tenth SPE comparative solution project: A comparison of upscaling techniques. In: SPE reservoir simulation symposium. Society of Petroleum Engineers (2001)
6. Collino, F., Ghanemi, S., Joly, P.: Domain decomposition method for harmonic wave propagation: a general presentation. Computer Methods in Applied Mechanics and Engineering **184**(2-4), 171–211 (2000)

7. Dolean, V., Gander, M.J., Veneros, E.: Asymptotic analysis of optimized Schwarz methods for Maxwell's equations with discontinuous coefficients. ESAIM: Mathematical Modelling and Numerical Analysis **52**(6), 2457–2477 (2018)
8. Dolean, V., Jolivet, P., Nataf, F.: An Introduction to Domain Decomposition Methods: Algorithms, Theory, and Parallel Implementation. SIAM (2015)
9. Gander, M.J.: Optimized Schwarz methods. SIAM Journal on Numerical Analysis **44**(2), 699–731 (2006)
10. Gander, M.J., Dubois, O.: Optimized Schwarz methods for a diffusion problem with discontinuous coefficient. Numerical Algorithms **69**(1), 109–144 (2015)
11. Gander, M.J., Kwok, F.: Best Robin parameters for optimized Schwarz methods at cross points. SIAM Journal on Scientific Computing **34**(4), A1849–A1879 (2012)
12. Gander, M.J., Magoulès, F., Nataf, F.: Optimized Schwarz methods without overlap for the Helmholtz equation. SIAM Journal on Scientific Computing **24**(1), 38–60 (2002)
13. Gander, M.J., Santugini, K.: Cross-points in domain decomposition methods with a finite element discretization. Electronic Transactions on Numerical Analysis **45**, 219–240 (2016)
14. Gerardo-Giorda, L., Le Tallec, P., Nataf, F.: A Robin-Robin preconditioner for advection-diffusion equations with discontinuous coefficients. In: Herrera, I., Keyes, D.E., Widlund, O.B., Yates, R. (eds.) 14th International Conference on Domain Decomposition Methods. Cocoyoc, Mexico (2002)
15. Greer, N., Loisel, S.: The optimised Schwarz method and the two-Lagrange multiplier method for heterogeneous problems in general domains with two general subdomains. Numerical Algorithms **69**(4), 737–762 (2015)
16. Gu, Y., Kwok, F.: Optimized Schwarz-based nonlinear preconditioning for elliptic PDEs. In: Domain Decomposition Methods in Science and Engineering XXV, pp. 260–267. Springer (2020)
17. Häberlein, F., Halpern, L.: Optimized Schwarz waveform relaxation for nonlinear systems of parabolic type. In: Domain Decomposition Methods in Science and Engineering XXI, pp. 29–42. Springer (2014)
18. Hughes, T.J.: The Finite Element Method: Linear Static and Dynamic Finite Element Analysis. Dover reprint, originally published in 1987 by Prentice-Hall, Englewood Cliffs, N,J. (2000)
19. Japhet, C., Nataf, F., Rogier, F.: The optimized order 2 method: application to convection–diffusion problems. Future Generation Computer Systems **18**(1), 17–30 (2001)
20. Lions, P.L.: On the Schwarz alternating method. iii: a variant for nonoverlapping subdomains. In: Third International Symposium on Domain Decomposition Methods for Partial Differential Equations, vol. 6, pp. 202–223. SIAM Philadelphia, PA (1990)
21. Lui, S.: A Lions non-overlapping domain decomposition method for domains with an arbitrary interface. IMA Journal of Numerical Analysis **29**(2), 332–349 (2009)
22. Maday, Y., Magoulès, F.: Non-overlapping additive Schwarz methods tuned to highly heterogeneous media. Comptes Rendus Mathematique **341**(11), 701–705 (2005)
23. Maday, Y., Magoulès, F.: Optimized Schwarz methods without overlap for highly heterogeneous media. Computer Methods in Applied Mechanics and Engineering **196**(8), 1541–1553 (2007)
24. Nataf, F.: Absorbing boundary conditions in block Gauss–Seidel methods for convection problems. Mathematical Models and Methods in Applied Sciences **6**(04), 481–502 (1996)
25. Nataf, F., Nier, F.: Convergence rate of some domain decomposition methods for overlapping and nonoverlapping subdomains. Numerische Mathematik **75**(3), 357–377 (1997)
26. Qin, L., Xu, X.: On a parallel Robin-type nonoverlapping domain decomposition method. SIAM Journal on Numerical Analysis **44**(6), 2539–2558 (2006)
27. Saad, Y.: Iterative methods for sparse linear systems, vol. 82, 2nd edn. SIAM, Philadelphia, PA (2003)
28. Toselli, A., Widlund, O.: Domain Decomposition Methods — Algorithms and Theory, vol. 34. Springer-Verlag (2005)